

Molecular Dynamics Study of the Nucleation of CH₄/C₂H₆ Binary Hydrate

by

Shuo Liu

A thesis submitted to the Faculty and the Board of Trustees of the Colorado School of Mines in partial fulfillment of the requirements for the degree of Master of Science (Applied Chemistry).

Golden, Colorado

Date: _____

Signed: _____
Shuo Liu

Signed: _____
David T. Wu
Thesis Advisor

Signed: _____
Amadeu K. Sum
Thesis Advisor

Golden, Colorado

Date: _____

Signed: _____
Thomas Gennett
Professor and Head
Department of Chemistry

ABSTRACT

Hydrates formed from CH₄/C₂H₆ gas mixtures have a practical significance since these gases are the main components of natural gas. Microsecond molecular dynamics simulations were performed to study hydrate nucleation and growth from CH₄/C₂H₆ gas mixtures under 600, 700 and 800 bar pressure and focused on the incipient stages of hydrate nucleation. Some aspects of the hydrate nucleation mechanism from CH₄/C₂H₆ mixtures can be observed from our results: the first cages to be formed are predominantly the 5¹² cages with CH₄, with C₂H₆ cages forming later. Increasing CH₄ concentration decreases the induction time, consistent with the observation that the first cage formed is usually with CH₄. By contrast, no strong effect of C₂H₆ concentration on induction time was observed. Higher pressure increases the nucleation rate, the cage diversity, the number of C₂H₆ molecules incorporated in the early cages and decrease the time to form the incipient hydrate cluster. Moreover, the stability of the cages with CH₄ increases with pressure, while the opposite trend is observed for cages with C₂H₆.

TABLE OF CONTENTS

ABSTRACT.....	iii
LIST OF FIGURES	vi
LIST OF TABLES	ix
ACKNOWLEDGMENTS	x
CHAPTER 1 INTRODUCTION	1
1.1 History of Hydrate Research.....	2
1.2 Motivation.....	3
1.3 The Structures of Clathrate Hydrates.....	7
1.4 Simulation Studies on Hydrate	9
1.5 Cooperative Adsorption Mechanism	15
1.6 Simulation Studies on Hydrate from Gas Mixtures.....	17
1.7 Experimental Studies on Hydrate from CH ₄ /C ₂ H ₆ Mixtures.....	19
1.8 Thesis Outline	20
CHAPTER 2 SIMULATION METHODS.....	22
2.1. Introduction.....	22
2.2. Molecular Dynamics Simulation	22
2.3 Simulation Details.....	24
2.4 MCG Order Parameter.....	26
CHAPTER 3 EFFECT OF GAS SOLUBILITY ON THE INDUCTION TIME.....	29
3.1 Abstract	29
3.2 Introduction.....	29

3.3 Calculation Methods	30
3.4 Results and Discussions	35
3.5 Conclusions.....	37
CHAPTER 4 THE INITIAL CAGES AND THE CAGE STABILITY.....	39
4.1 Abstract	39
4.2 Introduction.....	39
4.3 The Incipient Cages and Pressure Effects	42
4.4 Composition in Hydrate.....	44
4.6 The Cage Stability.....	46
4.7 Conclusions.....	53
CHAPTER 5 CONCLUSION AND FUTURE WORK	55
REFERENCES	61

LIST OF FIGURES

Figure 1.1	Cages and crystal structures of the most common clathrate hydrates; the 5^{12} cavity is common to all three structures as the "small cage", and is often called the building block of gas hydrates. The numbers adjacent to the various cages and setting off the arrows leading towards the different crystal structures indicate the number of each type of cage in one unit cell of the respective crystals. For example, a unit cell of sI hydrate contains two 5^{12} cages and six $5^{12}6^2$ ("large sI") cages, while a unit cell of sII hydrate contains sixteen 5^{12} cages and eight $5^{12}6^4$ ("large sII") cages. (Figure comes from Matt Walsh's Ph.D thesis).....	8
Figure 1.2	Two-dimensional example of one MCG monomer. A given minimum number of water molecules. N_w , must be within a specified angle ϕ of the guest-guest vector. The guests must be within distance R_{gcut} of each other, and the water molecules must be within distance R_{wcut} of each guest. Right: A typical structure that the MCG OP seeks to identify. Guests are represented in green and hydrogen bonds are represented in light red lines. (Figure comes from Walsh et.al ⁵⁴)	16
Figure 2.1	A simplified description of the standard classical molecular dynamics simulation algorithm. The flow chat is designed from the description on book by Frenkel and Smit. ⁹⁶	24
Figure 2.2	Left: Two-dimensional example of adjacency qualification for Mutually Coordinated Guests. A given minimum number of water molecules. N_w , must be within a specified angle ϕ of the guest-guest vector. The guests must be within distance R_g^{cut} of each other, and the water molecules must be within distance R_w^{cut} of each guest. Right: A typical structure that the MCG OP seeks to identify. Guests are represented in green and hydrogen bonds are visualized with light red lines between water molecules. (Figure comes from Barnes <i>et al.</i> , ^{58,59}).....	27
Figure 2.3	Schematic of MCG OP algorithm for a 2-D non-periodic system: (a) Initial configuration of guests (black dots) and water molecules (blue lines for qualifying clusters, blue dots for non-qualifying clusters). (b) Mutually Coordinated Guest monomers identified (green dots). (c) Neighboring monomers linked into clusters. (d) Example of clusters joined to form a larger cluster after a change in neighboring water configuration. (Figure comes from Barnes <i>et al.</i> , ^{58,59}).....	28
Figure 3.1	Schematic of the steps implemented to obtain nucleation simulations	31
Figure 3.2	An example of the potential energy curve of a hydrate formation trajectory:	

The snapshots from (a) to (e) show the evolution of the system (red and green dots represent the CH₄ and C₂H₆ molecules respectively. Red lines, green lines and yellow lines represent the cages with CH₄, C₂H₆ and empty cages. Water molecules are represented by the short gray lines). Before point a, the system was cooled down from the end of the previous NVT simulation and reach to the equilibrium metastable condition under the NPT simulation. Snapshot (a): the initial configuration for the system; Snapshot (b): the first cage was formed; Snapshot (c): the first 10 cages were formed. Snapshot (d) and Snapshot (e): the hydrate continues to grow till the end of the simulation. 32

Figure 3.3	Potential energy curve for hydrate formation runs under 255 K 600 bar.....	33
Figure 3.4	Potential energy curve for hydrate formation runs under 255 K 700 bar.....	33
Figure 3.5	Potential energy curve for hydrate formation runs under 255 K 800 bar.....	34
Figure 3.6	Typical profiles across the interface of the system showing the number density of CH ₄ (left) and C ₂ H ₆ (right).....	34
Figure 3.7	Bar plots showing the range of induction time within different ranges of methane (a) or ethane (b) concentration in water.	37
Figure 4.1	Fraction of different initial cages with CH ₄ (a) and C ₂ H ₆ (b) under different pressure (first 10 cages were counted in each trajectory), other cages with CH ₄ represent the uncommon ones: 4 ² 5 ⁸ 6 ³ , 4 ¹ 5 ¹⁰ 6 ³ ; for cages contains C ₂ H ₆ , the uncommon ones are 5 ¹² 6 ⁴ , 4 ¹ 5 ¹⁰ 6 ³ , 4 ¹ 5 ¹⁰ 6 ⁴ , 5 ¹²	43
Figure 4.2	The time (the average of all the hydrate-forming runs) to build the first 10 cages (blue bar), the time (the average of all the hydrate-forming runs) between the first cage and the first cage with C ₂ H ₆ (yellow bar) and the nucleation rate (red bar, the right y-axis) under different pressure.	44
Figure 4.3	The number of CH ₄ and C ₂ H ₆ in the largest MCG cluster in the hydrate phase at the initial stage of hydrate formation, the red line illustrates the point when the first cage was formed. 30 ns was counted before the red line and 100 ns was counted after. Case (a), CH ₄ outnumber C ₂ H ₆ ; Case (b), the number of CH ₄ is nearly the same as the number of C ₂ H ₆ ; Case (c), C ₂ H ₆ outnumber CH ₄ at the very beginning; the inserts illustrate the number of CH ₄ and C ₂ H ₆ in the largest MCG cluster for the entire simulation time	45
Figure 4.4	Two typical snapshots show the moment when the first cage with C ₂ H ₆ appeared under the low pressure (a) and high pressure (b). The thick blue	

cage represents the first cage with C₂H₆; red and cyan lines represent the completed cages with CH₄ and partial cages respectively. Red and green dots are used to represent CH₄ and C₂H₆. The number (average of all the trajectories) of completed cages (red bar) and partial cages (cyan bar) sharing the faces with the first cage with C₂H₆ that formed under different pressure. Here, we define partial cage as the one that has at least 6 faces. ... 46

- Figure 4.5 The formation process of a cage with C₂H₆ from a trajectory under 700 bar (we target the blue C₂H₆ molecule). Snapshot (a), the target blue C₂H₆ molecule and a red CH₄ molecule absorbed on either side of a single water ring composed by 5 water molecules. Snapshot (b), the target blue molecule started to form a cage near two partial cages with CH₄. Snapshot (c) to (d) the blue C₂H₆ molecule almost formed a cage but the cage is not stable, it exploded immediately. Snapshot (e) to (f), after the first failure of the attempt to form a cage, more 5¹² cages with CH₄ which are kinetics favorable, formed around the C₂H₆ molecule. Snapshot (g) to (h), the blue C₂H₆ formed a 5¹²6² cage and later, transformed into a 5¹²6³ cage. Movie 1 shows the whole process..... 47
- Figure 4.6 A cage with C₂H₆ formation progress illustrates in Fig.4.3 (c), which is a good example under high pressure (800 bar). Snapshot (a), a blue target C₂H₆ molecule and a red CH₄ molecule absorb on the either side of a ring composed by 5 water molecules. Snapshot (b), more water and guest molecules come together around the blue target C₂H₆ molecule. Snapshot (c), the blue and the pink C₂H₆ molecules begin to form the bowl-like partial cages. Snapshot (d), the blue C₂H₆ molecule formed a 4¹⁵10⁶2 cage, which is the first cage that formed in the system. Movie 2 shows the whole process. 47
- Figure 4.7 Cages fluctuate in the number of water molecules after formation. Figure 4.7 (a) and Figure 4.7 (b) come from Movie 3 and Movie 4 respectively..... 49
- Figure 4.8 The F _value for all the cages under different pressure (a) and different cages with different guest molecules (b); The error bars show the 95% confidence interval of the mean..... 51

LIST OF TABLES

Table 3.1	Hydrate formation runs under 255 K, 600 bar	35
Table 3.2	Non hydrate formation runs under 255 K, 600 bar	35
Table 3.3	Hydrate formation runs under 255 K, 700 bar	36
Table 3.4	Non hydrate formation runs under 255 K, 700 bar	36
Table 3.5	Hydrate formation runs under 255 K, 800 bar	36
Table 4.1	Cage diameter of the seven most dominated cages	49

ACKNOWLEDGMENTS

First and foremost, this thesis would not exist without the help from my committee. Thanks to Dr. David Wu, Dr. Amadeu Sum, Dr. Shubham Vyas, and Dr. Diego Gomez-Gualdron. The thesis cannot be finished within such a short time without your kind and timely help. I also want to thank Dr. Tina Voelker for her consistent help in my graduation by providing me financial support and useful guidance.

I also need to thank my family and my classmates for supporting me especially in my times of difficulty. Special thanks in this regard go to Dr. Caleb Tormey, Dr. Ben Zeidman, Dr. Michael Servis and Joe Maestas. Your suggestions for my research provided me many thoughtful ideas. I am very thankful for their feedback on many of my presentations, especially Joe who spent more than two days with me to modify my 560 seminar slides. Hanging out together with you guys has been one of my best memories. I wish Dr. Caleb Tormey, Dr. Ben Zeidman and Dr. Michael Servis all the best in your lives after you left here.

Most importantly, I really want to thank my thesis advisors Dr. David Wu and Dr. Amadeu Sum. I want to say thank you for all the time and efforts you spent on me on this research. Your wide scope of knowledge on the hydrate field and rigorous attitude toward science made me learn a lot, not only in the study of gas hydrate, but also to set a good example for me in terms of how to do research. I've always been grateful for the tolerance, patience and suggestions you gave me when I was making mistakes. I've become a better person during the past year and a half working together. Being one of your students is an honor of my life.

CHAPTER 1

INTRODUCTION

Clathrate hydrates (commonly referred to as gas hydrates, or simply hydrates) are ice-like solids that form when "guest" molecules such as methane (CH_4), ethane (C_2H_6), carbon dioxide (CO_2) and hydrogen (H_2) are trapped (enclathrated) inside hydrogen-bonded "host" water cages in a crystal lattice.¹⁻⁶ Low temperatures and high pressures are usually the conditions for hydration formation, though the formation conditions vary depending on the guest molecule.¹⁻¹⁵

Scientific curiosity, economic realities and environmental considerations have made research in gas hydrates draw the attention from scientists of different backgrounds, including geology, chemistry, environmental, chemical and petroleum engineering. The huge amount of natural gas in hydrate reservoirs in nature not only might have huge effects on the global climate, but also can be considered as a promising kind of potential clean energy resource. In the oil industry, crude oil pipelines are commonly operated under low temperatures and high pressures, which are thermodynamic conditions for hydrate formation. As a result, the formation of hydrate from natural gas and water contained in crude oil is a significant threat in flow assurance. Some new technologies are also based on the formation of hydrate, such as gas separation and gas transportation. Considering the wide interdisciplinary aspects of gas hydrates, only one paper or one thesis certainly cannot cover them all. This thesis helps to answer two fundamental questions regarding hydrates from a chemistry perspective with the help of computer simulation: what is the mechanism of hydrate formation from a gas mixture,

and how does the hydrate formation vary under different conditions.

In the remainder of this chapter, I will introduce the history and the motivation of hydrate study. After that, the structure of gas hydrates will be introduced. I will then give an overview of the application of computer simulation in the study of hydrates. Finally I will review previous theoretical and experimental studies on hydrate formation from gas mixtures.

1.1 History of Hydrate Research

The research history of hydrate spans more than two hundred years. Sir Humphry Davy is believed to be the first person who discovered hydrate in the early 1800s.² He observed an ice-like solid forming at temperatures above the freezing point of water composed of more than just water. In 1823, the first quantitative investigations of hydrate were made by Michael Faraday by measuring the composition of chlorine hydrates.^{1,3}

Following the introduction by Sloan,¹ research efforts on natural gas hydrates can be classified into three landmark phases. The first period starting from their discovery, includes gas hydrates as a scientific curiosity. Early efforts in this period were mainly focused on searching for different kinds of hydrate formers and the conditions for hydrate formation. The second period, starting from 1934, predominantly concerns man-made gas hydrate as a hindrance to the natural gas industry. The third period, from the mid-1960s till the present, began with the discovery that nature predated man's fabrication of hydrates by millions of years, *in situ* in both the deep oceans and the permafrost regions as well as in extraterrestrial environments.

1.2 Motivation

The research of gas hydrate has drawn the attention from a considerable number of scientists in different fields. Natural reserves of gas hydrate in the earth can supply natural gas as a source of energy. Large quantities of gas hydrates exist in the world's permafrost areas and continental margins, where the temperature, pressure and chemical conditions are appropriate for hydrate formation.⁴ Even by the most conservative estimates, the energy dormant in terrestrial deposits of gas hydrates (predominantly in the form of enclathrated methane) is approximately double that of all known conventional fossil fuel (coal, oil and conventional natural gas) combined. The amount of methane estimated to be *in situ* gas reserves is approximately 10^{16} m^3 .^{10,11} The energy demands of the United States for the next eight decades could be satisfied by only 1% of the estimated reserves of methane hydrate.¹² Thus hydrates have been widely considered as a potential source of energy.⁴⁻⁶

Gas hydrate in nature may have a huge effect on the earth's environment.⁶ Since methane hydrates can be stable only under very specific conditions, it is conceivable that global warming, which as a matter of fact includes the temperature increase of the oceans, could affect the stability of gas hydrates. Climatic changes in the past could have led to the destabilization of methane hydrates and thus to the feedback release of methane, a potent greenhouse gas. Evidence of this global climate change period in earth's history was reported by Kenett et al.⁷

In the oil and gas industries, hydrocarbon transportation pipelines containing oil, natural gas, condensate and water, are regularly operated at low temperatures and high pressures that are thermodynamically suitable for hydrate formation. The formation of hydrate is the main

obstacle to uninterrupted fluid flow in oil and gas pipelines. Thus, the task of eliminating or controlling hydrate formation is among the costliest in the growing field of flow assurance engineering. Current practice is to add sufficient amounts of thermodynamic inhibitors such as methanol and ethylene glycol into the water phase to increase the temperature of hydrate formation, i.e. by shifting the phase boundary. But due to the large volumes of thermodynamic inhibitor that are needed, the cost is high and becoming more and more economically untenable.^{1,6} As a result, controlling the time-dependent properties of hydrate formation by adding low dosage hydrate inhibitors (LDHIs) is becoming a new way that can potentially replace the traditional method of injecting huge amounts of thermodynamic inhibitor. The LDHIs that have been developed can be divided into two basic categories: kinetics inhibitors, that retard the formation or growth of gas hydrates, and anti-agglomerants, that prevent small hydrate particles from coalescing into larger agglomerates.^{1,6} Compared to the study of time-independent thermodynamics properties, studies on time-dependent properties of hydrate formation are more complicated. As a result, developing relevant functional molecules that will be appropriate additives that can affect the time-dependent properties of hydrate has become an important area of research.

Other than in pipeline flow assurance, gas hydrate has many potential applications such as gas storage, gas transportation and gas separation.^{1,6,13,15} Several studies have shown that the gas hydrate structures have considerable potential as storage media for various gases (for instance, they can be used for natural gas/hydrogen storage and transportation), as well as the cooling storage media in air conditioning systems, etc.¹⁴⁻²⁰ Compared with conventional means of gas storage methods such as liquefaction, storage and transportation in the form of

gas hydrate have a safety advantage for the corresponding processes, as well as much lower process volumes in comparison with other methods.²¹ Because of the lower investment needed in infrastructure and equipment, the capital cost for natural gas transportation in the form of gas hydrates is projected in detailed economic studies to be lower than that for liquefied natural gas (LNG) over a significant range of transportation distances.^{22,23} However, the transportation of gas as LNG is currently preferred for long distance markets or transportation of natural gases produced from huge gas fields.²⁴ On the other hand, there is evidence, for instance from the Mitsui Ship Building & Engineering Company Pilot Plant in Hiroshima, Japan, that gas hydrate can in some conditions be economically more cost effective for storage and transportation of standard gas compared to the LNG methods.²⁵ In particular, this new method of gas transportation using the formation of hydrate is advantageous when the position of delivery is far from the pipeline and the required quantity is not too large. Strobel and coworkers published a comprehensive review on the application of gas hydrate for hydrogen storage²⁶ and Chatti et al have discussed the use of gas hydrates as a thermal working medium in air conditioning processes.²⁷

Gas separation is another potential application for gas hydrate, such as CO₂ separation and CO₂ capture. The capture and sequestration of CO₂ (CCS) has become an important area of research to mitigate CO₂ worldwide.²⁸⁻³⁰ Evaluating and developing energy efficient and environmental friendly technologies to capture the CO₂ produced in large scale power-plants remains a challenge, where CO₂ and N₂ are the main components in the flue gas. Hydrate crystallization techniques can be one novel approach to separate CO₂ from combustion flue gas.^{28,29} When hydrate crystals are formed from a binary mixture of these gases, due to the

difference in affinity between CO₂ and other gases, the hydrate phase is enriched in CO₂ while other gas species are enriched in the gas phase. Depressurization and heating can later be used to dissociate the hydrate phase and recover CO₂. CO₂ selectivity in the hydrate phase could be more than four times higher than that in the previous gas phase based on the results of experimental studies.³¹ Hydrate formation based gas separation processes usually need chemical additives as promoters. The function of these promoters are generally to reduce the required hydrate formation pressure and increase the formation rate and/or temperature, as well as modifying the selectivity of hydrate cages to absorb various gas molecules. Gas hydrate formation promoters can be categorized into two groups based on whether or not the chemical additives can change the hydrate structure. Tetrahydrofuran (THF), anionic/non-ionic surfactants, cyclopentane, acetone etc. belong to the first category which does not affect the structure of water cages,^{32,33} while tetra-n-butylammonium salts and [(n-C₄H₉)₄NBH₄] belong to a second category that do change the water cages in the traditional clathrate structures.^{34,35}

All these potential environmentally friendly hydrate-based technologies rely on the formation of hydrates for their implementation. Besides, a comprehensive understanding of the time-dependent properties of hydrate can provide a basis for the molecular design of new generations of LDHIs. As a result, a comprehensive understanding of the mechanism of how hydrates form, especially from gas mixtures, could help engineers and scientists to manipulate these processes and bring them to reality with economic viability.

In this thesis, the nucleation mechanism of binary hydrate from CH₄ and C₂H₆ was studied by molecular dynamics simulation. The composition of typical natural gases has been

quantified in oil and gas production by several studies:^{1,6,8,79} more than 85 mol% is CH₄, with C₂H₆ and higher paraffins comprising the balance. Since CH₄ and C₂H₆ are the two major components of natural gases, hydrates formed from these gases are of practical significance. Understanding the nucleation mechanism of binary hydrate from CH₄ and C₂H₆ will be helpful to provide some potential strategies for the development of future LDHIs.

1.3 The Structures of Clathrate Hydrates

Depending on the guest molecules present and the local thermodynamic conditions, gas hydrates form a variety of crystalline structures. Similar to ice, the hydrogen bond is the basis for water molecules bonding in tetrahedral structures. Pentagonal and hexagonal water clusters formed by hydrogen bonds are also frequently found in water. All common natural gas hydrates belong to the three crystal structures, cubic structure I (sI), cubic structure II (sII), or hexagonal structure H (sH).¹ The sI unit cell is composed of two pentagonal dodecahedron (5^{12}) cages and six tetradecahedron ($5^{12}6^2$) cages; the sII unit cell contains sixteen 5^{12} and eight hexadecahedron ($5^{12}6^4$) cages and the sH unit cell contains three 5^{12} , two $4^35^66^3$, and one $5^{12}6^8$ cage.¹ The cages in the common structures of gas hydrates all contain even numbers of water molecules and obey Euler's formula for convex polyhedra,^{8,9} in which the Euler Characteristic X ($X = F + V - E$, or number of faces (F) plus number of vertices (V) minus number of edges (E)) is equal to two. For example, the 5^{12} cage contains 12 faces, 20 vertices (water molecules), and 30 edges (hydrogen bonds), and thus its Euler Characteristic is two ($12 + 20 - 30 = 2$). Figure 1.1 shows the cages comprising the three most common

types of gas hydrates.

A cavity common to these hydrate structures is the pentagonal dodecahedron 5^{12} cage, which is connected through its vertices to form sI hydrate, through face-sharing in three dimensions to form sII hydrate, or through face-sharing in two dimensions to form connecting layers in structure H. The spaces between the 5^{12} cages are the larger cages: oblate $5^{12}6^2$ cages in sI hydrate or the spherical $5^{12}6^4$ cages in sII. In sH hydrate, both $5^{12}6^8$ and $4^35^66^3$ cages form between layers of 5^{12} cages.

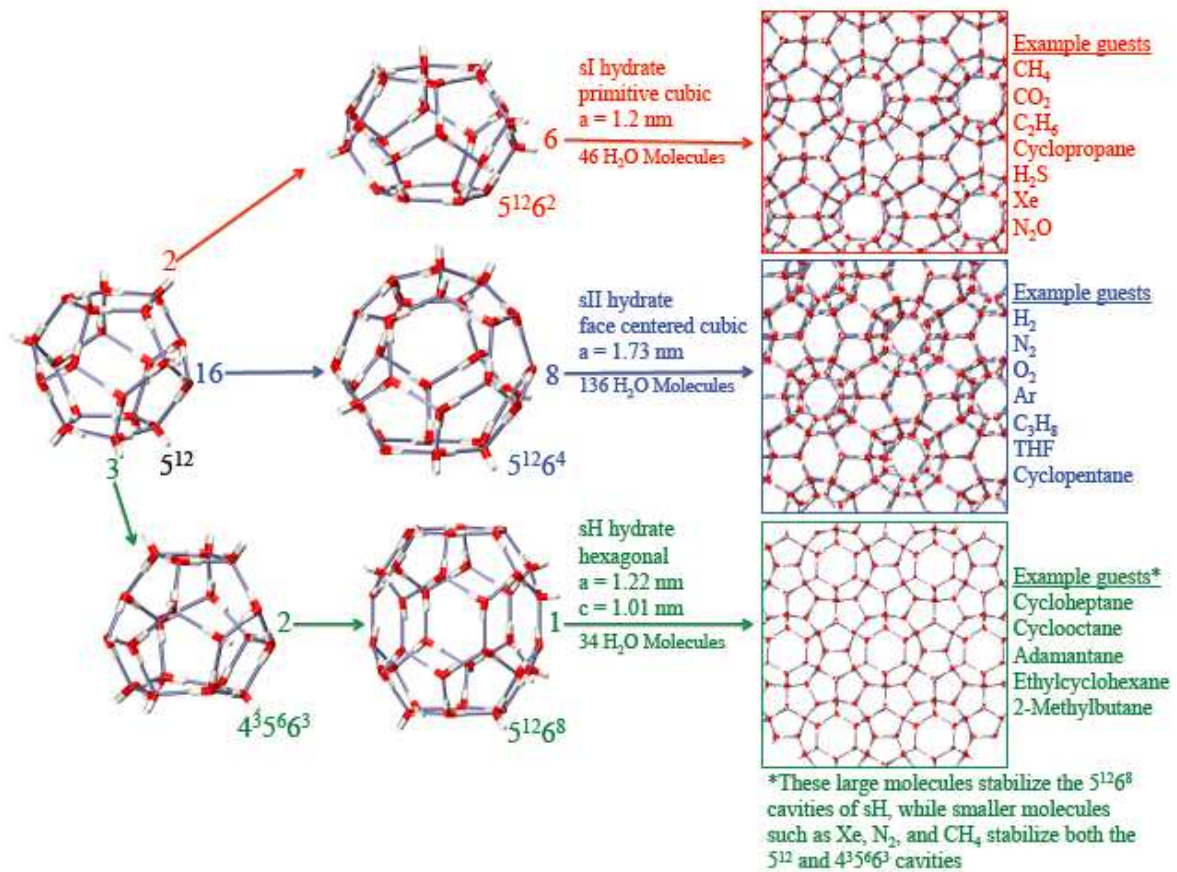


Figure 1.1 Cages and crystal structures of the most common clathrate hydrates; the 5^{12} cavity is common to all three structures as the "small cage", and is often called the building block of gas hydrates. The numbers adjacent to the various cages and setting off the arrows leading towards the different crystal structures indicate the number of each type of cage in one unit cell of the respective crystals. For example, a unit cell of sI hydrate contains two 5^{12} cages and six $5^{12}6^2$ ("large sI") cages, while a unit cell of sII hydrate contains sixteen 5^{12} cages and eight $5^{12}6^4$

("large sII") cages. (Figure reproduced from Matt Walsh's Ph.D thesis)

Different molecules can fit different cages. The hydrate structure is determined by the guest size to a large degree. The size ratio of the guest to cavity guides the determination of crystal structure and cage occupancy, which in turn, determines equilibrium pressures and temperatures for the hydrate phase. Small molecules usually occupy the small cages, but can also occupy the large ones. By occupying the large cavity, large molecules (such as propane or carbon dioxide) can stabilize sI or sII hydrates, while leaving the smaller cavity vacant. Both large and small cavities must be occupied for sH hydrate. The hydrate cage structure is stabilized by the repulsive interactions (hydrophobic property of guest molecules) between guests and hosts molecules. ¹

1.4 Simulation Studies on Hydrate

Due to its fine resolution in both time and space and its ability to follow the nanoscale trajectories of individual molecules, computer simulation is a powerful tool in the investigation of hydrate in many aspects such as nucleation,³⁶⁻³⁹ surface phenomena⁴⁰⁻⁴⁴ and hydrate growth.^{45,46}

Studies on the formation mechanism have been carried out from experiments to computer simulations. Radhakrishnan and Trout proposed the "local structure" hypothesis that suggested guest molecules arrange into a hydrate-like configuration and perturb the structure of water molecules nearby.⁴³ Hydrate formation can then occur when the number of locally ordered guest molecules exceeds the critical nucleus. A free energy calculation

showed it is thermodynamically more favorable for the labile clusters to disintegrate than to agglomerate, contradicting the previous hypothesis by Sloan and coworkers which suggested that “labile clusters” of water formed around guest molecules in solution agglomerate into a critical hydrate nucleus.^{48,49} Moon *et al.* proposed a similar model on the basis of a short timescale molecular dynamics (MD) simulation of CH₄ hydrate nucleation,⁵⁰ and supported the locally structuring hypothesis. Other mechanisms such as cage adsorption⁵¹ and the blob mechanism^{52,53} were also proposed. The cage adsorption mechanism indicated an important role for a completed water cage in terms of attracting more methane molecules, with the method of the calculation of the potential of mean force (PMF). The proposed blob mechanism involves the reversible formation of a long-lived amorphous cluster of water-separated guests (blob), wherein the blob of hydrate cages reaches a critical size that prompts hydrate growth. Walsh *et al.* reported the first unconstrained MD simulation of CH₄ hydrate nucleation on a microsecond timescale in 2009. The locally ordered structure with the CH₄ absorbed on the bowl-like and face-sharing partial cages formed by water molecules initiates the hydrate formation.⁵⁴ The cooperative adsorption mechanism was also proposed. Order parameters (OPs) are used to quantify the hydrate nucleation and growth. The most commonly used OPs are the potential energy, the angular order parameter (AOP), the four-body structural order parameter (F₄) and the number of water molecules in the largest cluster (H-COP).⁵⁵⁻⁵⁷ Based on the observations made by Walsh *et al.*,⁵⁴ a new order parameter that combined both guest and host molecules called “mutually coordinated guests” (MCG)⁵⁸ was developed and used to determine the critical nucleus size by advanced sampling methods such as p_B histogram and equilibrium path sampling.⁵⁹ MCG-1 was used as

an accurate quantitative descriptor for the molecular mechanism for methane hydrate nucleation at 255 K and 500 bar. A nucleation pathway was observed in which initial structures leading to the critical nucleus contain both partial and complete hydrate cages but are not defined by a crystalline structure. From equilibrium path sampling calculations, MCG-1=16 was determined to be the critical nucleus under the conditions of the simulation.⁵⁹

It is worthwhile noting that, while experimental investigations are thought likely to investigate heterogeneous nucleation due to impurities which cannot be totally removed as well as due to experimental apparatus surfaces, the simulation studies on hydrate nucleation mentioned above occur in the absence of a surface or impurities. There is the gas-liquid interface, but it is still unclear whether it plays a role in the nucleation process, and so the simulation studies may correspond to homogeneous nucleation. A study by Bai *et al.* reported the kinetic pathway of CO₂ hydrate formation triggered by hydroxylated silica surfaces.⁶⁰ The process of CO₂ hydrate formation on the surface was characterized by three stages, including the formation of an ice-like layer near the substrate, followed by the formation of an intermediate structure layer. Based on this intermediate layer sharing similarities with both ice and hydrate that formed during stage two, CO₂ hydrate is then generated. The presence of an existing solid template may encourage the formation of immediate crystallinity, which provides a possible explanation for the gap (the conditions of hydrate formation) between the experimental studies and the simulation, since much higher driving forces are necessary to form hydrate in the simulation studies.

One primary goal of simulation studies on hydrate surfaces and hydrate growth is to

investigate the mechanism of hydrate inhibitor or the effects of other chemicals on hydrates. Anderson *et al.* studied the effects of four common types of hydrate kinetic inhibitors (poly(*N*-vinyl-2-caprolactam) or PVCap, polyvinyl pyrrolidone (PVP], polyethylene oxide (PEO) and *N*-methyl-*N*-vinylacetamide (VIMA) on hydrate interfaces.⁴³ The results suggested that, the mechanism of kinetic inhibitors can be attributed to their disruption of the organization of water molecules nearby the hydrate interface, which defers the growth of hydrate from the existing surface. The effectiveness of different inhibitors can be evaluated by how strong the interactions are between the inhibitor and the liquid water phase under hydrate-forming conditions. In other words, the formation of strong hydrogen bonding between the inhibitor molecule and the hydrate surface is crucial. In terms of molecular structure, strong bonding can be expected when the inhibitor has a charge distribution on the edge similar to the charge separation in the water molecules on the surface of the hydrate as well as having a similar size to the available space at the hydrate-surface binding site. This conclusion could be a useful guide to future kinetic hydrate inhibitor design. Yagasaki and coworkers studied a commonly used hydrate kinetic inhibitor, PVcap. Strong bonding can be observed when PVcap monomer adsorbs on the hydrate surface, which supported the previous discovery by Anderson *et al.*⁴³ The simulation results indicated that entropic stabilization arising from the presence of cavities at the hydrate surface is a possible reason for the preference of PVcap on the hydrate surface.⁴⁴

Vatamanu *et al.* studied CH₄ hydrate growth in the presence of an appropriate crystal template. A strong tendency for water molecules to organize into cages around CH₄ at the growing interface was observed and the interface also demonstrated a strong affinity for CH₄

molecules.⁶¹ Yagasaki *et al.* studied the growth of ethylene oxide (EO) and tetrahydrofuran (THF) hydrate.⁴⁵ The growth rate of THF hydrate is even slower than ice because THF molecules prefer the open small cages at the hydrate surface, which is the reason for the inhibition of the growth of THF hydrate. By contrast, the growth rate of EO hydrate is an order of magnitude higher than that of THF hydrate.⁴⁶

The interfacial curvature of the gas phase in coexistence with liquid has been found to have a profound effect on the concentration of dissolved CH₄, and can thus greatly affect the nucleation rate.⁶² For instance, much higher applied pressure (at least one order of magnitude higher) is needed for simulations with a flat methane-water interface compared with curved (spherical or cylindrical) interfaces at the same temperature under the same ensemble. While the fluctuations involving surface cage destruction and reformation are expected given the highly dynamic nature of hydrogen-bonded systems, the cage transformation is pretty common in the hydrate system.⁶³ Two types of mechanism of cage transformation were concluded by Walsh *et al.*: water molecule insertion/removal, which increases or decreases the number of water molecules in a cage, and water rotation, which does not change the total number of water molecules in the cage. Compared to systems with little long-range hydrate order, trajectories with long-range hydrate order have higher $5^{12}6^2/5^{12}$ and $5^{12}6^3/4^15^{10}6^2$ cage ratios.⁶³ Multiple pathways of hydrate nucleation can be observed. Liang *et al.* studied H₂S hydrate formation in a constant energy simulation and found rapid formation of amorphous hydrate-like structures that could subsequently anneal to crystalline solids.⁶⁴ However, Zhang *et al.* studied CH₄ hydrate nucleation in the microcanonical ensemble in the absence of a thermostat. sI-like hydrate structure with long-range order spanning the simulation box across

the periodic boundaries was observed, which indicated that, gas hydrate can nucleate not only to amorphous solids, but can also nucleate directly to the ordered solid with a high degree of crystallinity,⁶⁵ which provided another possible pathway for hydrate nucleation.

All the papers reviewed above are for hydrate formation from CH₄, while Wilson *et al.* studied hydrate formation from C₂H₆.⁸⁰ Due to the difference in size, comparing with CH₄, C₂H₆ molecules tend to occupy larger cages (such as 4¹5¹⁰6², 5¹²6²) rather than the 5¹² cage which is the most prevalent cage in the methane hydrate system. The 4¹5¹⁰6² metastable cage with an oblong shape, though not the type of cage in the hydrate crystal structure, can be found frequently in the system. The 4¹5¹⁰6² metastable cage prefers to be the first cage to appear in the formation of C₂H₆ hydrate. Cage transformation phenomena can also be observed similar to the observations made by Walsh previously. The kinetically favorable cages such as the 4¹5¹⁰6² cage can transform into thermodynamically favorable cages such as 5¹²6² and 5¹². The 4¹5¹⁰6² cage tends to transform into 5¹²6² more often than 5¹² because the volume of the 5¹² cage is too small to accommodate C₂H₆. The 5¹² empty cage can also be found. The orientation of the guest C₂H₆ molecule displays a clear preference for an orientation along the axis of the square face, undergoing hindered rotation with 180 degree flips, and following the square face location if it relocates due to cage reorganization.

Published simulation articles on hydrates are mainly based on molecular dynamics simulations. Studies based on other computational methods such as Monte Carlo or first principle methods are not that common. Brumby *et al.* performed isobaric-isothermal Gibbs ensemble Monte Carlo simulations of sI CH₄ hydrates in equilibrium with bulk CH₄ to calculate the large and small cage occupancies.⁶⁶ The cage occupancy results showed good

agreement with the cage occupancy predictions obtained using CSMGem, which was based on the solid solution model by van der Waals and Platteeuw. Liu *et al.* performed ab initio calculations to investigate the formation process of clathrate cages of sI CH₄ hydrate.⁶⁷ In accord with the results of a previous molecular dynamics study,⁵⁴ the cage precursor of the hydrate formation is one pentagonal ring of water molecules plus one guest molecules for the small cages. From the stabilization energy calculations, the formation of larger cages (larger than a 5¹² cage) is more thermodynamically favorable than that of 5¹² cages, which contain only 20 water molecules, due to the higher number of hydrogen bonds.

1.5 Cooperative Adsorption Mechanism

As mentioned above, Walsh *et al.* first reported the first unconstrained MD simulation of CH₄ nucleation on a microsecond timescale in 2009.⁵⁴ Figure 4.7, reproduced from the publication of Walsh *et al.*, illustrates the nucleation process of methane hydrate, which is useful to understand the cooperative adsorption mechanism.

From snapshot A, at 1.139 μ s, we can see five water molecules adsorb two orange methane molecules which is the initial structure of the hydrate formation. With the methane molecules adsorbed on opposite sides of a single planar pentagonal ring composed by five water molecules, due to their hydrophobic property, more methane molecules nearby can be more ordered. The ordered water molecules can form cage-like patterns which will adsorb more methane molecules and protect the incipient hydrate cluster from dissociation. The lifetime of the faces of bowl-like partial hydrate cages will be prolonged by the more

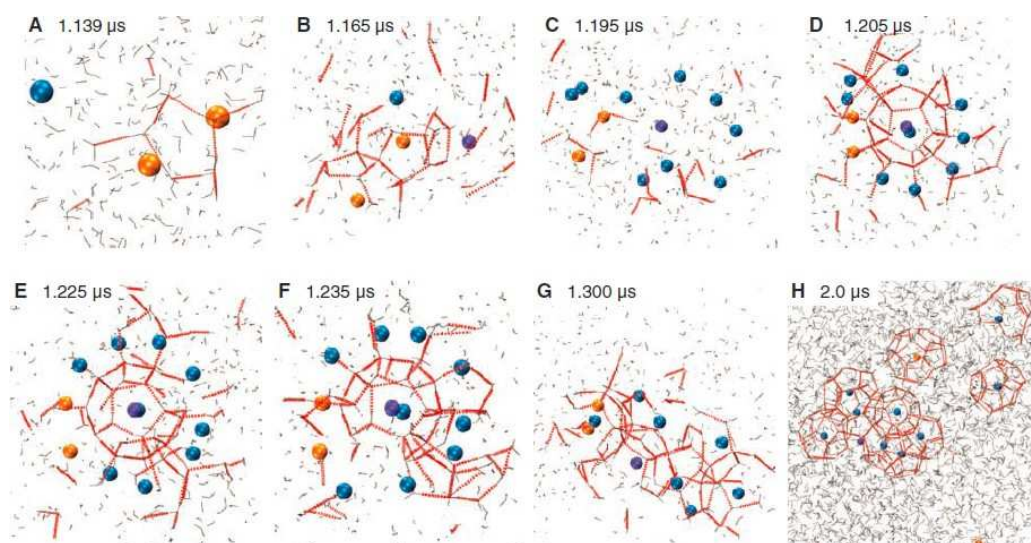


Figure 1.2 The formation process of methane hydrate. (A to C) A pentagon formed by five water molecules attracts two methane molecules. The initial structure formed by water and methane later grows into bowl-like partial cage patterns. This bowl-like partial cage patterns are not stable, and it dissociate after several nanoseconds. (D and E) The first cage which is a 5^{12} cage forms with eleven to twelve methane molecules adsorbed on the surface. (F and G) The 5^{12} cage opens to the formation of a network of face-sharing cages, which favors the growth of hydrate. (H) A snapshot of the system after hydrate growth. (Figure comes from Walsh *et.al*⁵⁴)

methane molecules. Surrounded by a bowl-like pattern in the first shell of adsorbed methane molecules, that process leads to the gradual formation of a first completed small 5^{12} cage at 1.225 μ s. However, that newly formed cage is not stable with a lifetime only about 30 ns. The newly formed 5^{12} cage opens and breaks. With the formation of more and more newly formed cages, the hydrate cluster becomes more stable and forms a non-disappearing hydrate phase in the end.

Based on the process of hydrate formation, the cooperative adsorption mechanism was proposed and has been reported in many studies. In this mechanism, at the beginning, the planar water faces connected by hydrogen bonds absorb guest molecules, due to the hydrophobic property of methane, water molecules will form cage-like rearrangement around

these adsorbed guests, which in turn protect the incipient hydrate cluster from dissociation and favor the further growth of hydrate. This process eventually leads to the formation of a full cage which provides more guest adsorption sites and promote the hydrate formation. This positive-feedback mechanism is the reason why the process is called "cooperative", which can lead to the formation of a large enough solid under the conditions of interest in the end.

1.6 Simulation Studies on Hydrate from Gas Mixtures

Recently, more simulation studies have focused on hydrate nucleation from a gas mixture rather than a single component. He *et al.* studied hydrate nucleation from a CO₂ and CH₄ gas mixture.⁶⁸ Similar to the CH₄ hydrate nucleation mechanism made by Walsh *et al.*,⁵⁴ CO₂ and CH₄ cooperatively adsorb to hydrogen bonded water rings leading to hydrate-like ordering and cage formation and the 5¹² small cage with CH₄ initiates the formation. Due to the difference in sizes, CO₂ and CH₄ prefer to occupy different cages: in the incipient hydrate, CH₄ prefers to occupy 5¹², 4¹5¹⁰6² and 5¹²6² cages, while CO₂ prefers to occupy 4¹5¹⁰6² and 5¹²6² cages. Short-range order of sI and sII motifs can also be found. CO₂ can increase the hydrate formation rate due to its high solubility. Wu *et al.* studied the hydrate formation from THF and CH₄ and a comparison was made with the pure system.⁶⁹ Mutual cooperative effects of THF and CH₄ can be observed. Though the high solubility of THF provides enough guest molecules in the aqueous phase, due to the highly dynamical nature of hydrogen bonding between THF and water, hydrate cage structure cannot be easily formed. In contrast, the presence of CH₄ in the THF solution can more readily form hydrate cages. These cages

formed by CH₄ (mainly 5¹²), can provide support for THF to form large 5¹²6⁴ cages. The introduction of CH₄ provides stable 5¹² cages, and as a result, a non-disappearing cluster of cages can be formed within a significantly shorter amount of time. Hall *et al.* studied hydrate nucleation from a CH₄ and hydrogen sulfide (H₂S) gas mixture and demonstrated, in an analogy to protein folding and self-assembly, the potential energy landscape of hydrate nucleation is also funnel-shaped with multiple pathways and kinetics traps.^{70,71} The solution composition was shown to not be the sole determinant of guest enclathration rates. Due to the highly dynamical nature of aqueous phase, non-standard cages were revealed at the interface between the hydrate nucleus core of the aqueous phase with a key factor affecting guest enclathration rates. Hydrates formed from all the above four binary hydrate systems have practical significance: studies on hydrate formation from CH₄/CO₂ system will be helpful to understand the mechanism for using CO₂ to replace natural gas in a hydrate reservoir under the sea or providing strategies for hydrate based technologies for CO₂ separation. THF is not only a common additive as a thermodynamic promoter in hydrate studies, but also can form sII hydrate by itself. Thus, the study of hydrate formation from this binary mixture can be useful to illuminate how a second molecule may affect the nucleation process. H₂S is the main component in high sulphur containing gas fields, such as those in Alberta, Canada. As a result, the study of hydrate formation from CH₄/H₂S is important for gas production from high sulphur containing natural gas fields. In this thesis, hydrate formation from CH₄/C₂H₆ mixtures, which are the main components of natural gas, will be helpful to understand the hydrate formation mechanism in pipelines and could potentially provide guidelines for the development of LDHIs.

1.7 Experimental Studies on Hydrate from CH₄/C₂H₆ Mixtures

Both experimental and modeling are important for future hydrate research. Understanding the nature of CH₄ and C₂H₆ binary hydrate formation, including metastability, is important for the oil and gas industry since the formation of sI and sII mixtures and the subsequent interconversion from a metastable to a stable structure are likely to occur in the pipelines. Experimental tools, both microscopic (X-ray diffraction, Raman, NMR etc) and macroscopic (gas uptake measurements, morphology etc), are useful to identify and analyze the relevant phases.⁷² Subramanian *et al.* used Raman and NMR spectroscopic measurements on CH₄ and C₂H₆ mixture hydrates and found evidence of sII hydrates forming within certain composition ranges. Later, they demonstrated a trace amount of C₂H₆ (about 0.005-0.008 mole fraction in the gas phase) can be sufficient to drive the hydrate structure from sI to sII.⁷³ Moreover, the coexistence of multiple structures at pressures above incipient formation conditions can be found from the phase diagram. CH₄-C₂H₆ gas mixtures can form sI hydrate with the CH₄ concentration up to 75% or higher than 99% in the gas phase. The mixtures can also form sII structure with the CH₄ concentration ranging from 75%-99%.⁷⁴ The formation of sII hydrate from two sI hydrate formers can be attributed to the abundance of small cavities in sII hydrate that can be stabilized by CH₄ and the reduced competition between CH₄ and C₂H₆ for the occupation of large cavities in the hydrate. The two structures usually coexist as a metastable state when the gas composition is close to the sI/sII phase boundaries.^{1,73,74} Ohno *et al.* studied the metastability of CH₄ and C₂H₆ mixture hydrate and found out that a commonly used kinetic hydrate inhibitor, PVcap, had the opposite effect in terms of affecting the metastability of sI and sII hydrate.⁷⁵ The faster conversion of hydrate

structure can be observed at higher CH₄ concentration. Naeiji *et al.* studied the hydrate separation effects from CH₄ and C₂H₆ gas mixtures and demonstrated the two gases were fully separated at low and high mole fractions of CH₄ in the gas phase.⁷⁶

Schicks and coworkers used *in situ* Raman spectroscopy, microscopic observation, and *in situ* X-ray diffraction to observe the formation process of CH₄ hydrate and mixed hydrate.^{77,78} In accord with the simulation result,⁵⁴ the first step to initialize the hydrate is the formation of a pentagonal dodecahedron cage (5¹²) with CH₄, while the formation of all other cavity types with other guest molecules (in this study, CO₂, H₂S, C₃H₈, 2-methylpropane and 2-methylbutane) occurs later. The incipient hydrate phase is not highly crystalline, which may be consistent with the blob hypothesis^{52,53}, which suggests the amorphous structure could be a precursor of hydrate. However, we emphasize that nucleation occurs at a much smaller size scale than is detectable by experiment, and so these parallels can only be suggestive. The composition of the hydrate phase differs from the gas phase, reflecting gas separation effects of the formation of hydrate.⁷⁷ The cage occupancy of different molecules was also studied with time-resolved Raman spectroscopy. Different molecules preferred incorporation into different cavities in the various hydrate structures. Competition in cage occupancy between different molecules were observed, for instance, H₂S seemed to inhibit the incorporation of CH₄ into the 5¹²6² cavities.⁷⁸

1.8 Thesis Outline

In this thesis, we performed microsecond MD simulations to study the nucleation and

growth of CH₄/C₂H₆ mixture hydrate and focus on the initial stage of hydrate formation. Based on the previous simulation results on pure CH₄ and C₂H₆ hydrate system, difference in cage preference can be found out and the oblong shaped 4¹5¹⁰6² cage is the first one formed and most prevalent in the pure C₂H₆ system which is different from the pure CH₄ system,⁸⁰ where 5¹² cage is most prevalent and initializes hydrate formation.^{54,62} Some similarities and differences can be compared between the mixture system and the pure system. Our simulation results will be helpful to understand the hydrate nucleation mechanisms of gas mixtures as well as the role of different guest molecules.

The outline of the thesis is presented as follows. Chapter 2 introduces molecular dynamics simulation, which is the main tool used in this thesis, and its application to the study of gas hydrate formation, with all the simulations details. The MCG order parameter will also be introduced. Chapter 3 presents the results of the effect of aqueous guest concentrations on the induction time. In Chapter 4, we focus on the effect of pressure on the incipient cages and their stabilities. In Chapter 5, the conclusions of this thesis are revisited along with suggestions for future study.

CHAPTER 2

SIMULATION METHODS

2.1. Introduction

Due to its fine resolution in both time and space and its ability to follow the nanoscale trajectories of individual atoms, molecular dynamics (MD) simulation is the main method used in this thesis to study hydrate nucleation. As mentioned in Chapter 1, MD simulation has been a popular technique for gaining insight into hydrate nucleation, surface phenomena as well as hydrate growth. In this chapter, we first compare the differences between the two most common simulation methods: molecular dynamics and Monte Carlo (MC) simulation, and later, provide details of the MD simulation methods that were used through this study. Some further technical details in this study are also clarified, such as how to determine the hydrate cluster and how to determine the induction time. The Mutually Coordinated Guests (MCG) order parameter, which involves both guest and host molecules in the hydrate, can be used to quantify hydrate nucleation and growth. The algorithm defining the MCG order parameter is also presented in this chapter. By using the idea of the MCG order parameter, the hydrate phase can be identified by searching for MCG monomers in the box and the result of this part will be shown in Chapter 4.

2.2. Molecular Dynamics Simulation

Molecular dynamics (MD) is a computer simulation method for studying the physical movements of atoms and molecules based on Newtonian Mechanics. The method was

originally developed within the field of theoretical physics in the late 1950s, but is applied today mostly in chemical physics, materials science and the modeling of biomolecules.

MC and MD simulations are the two main types of molecular simulation methods. The basic idea of MC simulation is to generate a series of random configurations to compute average properties. Each configuration is weighted with the normalized Boltzmann factor. The criterion for the system to "accept" or "reject" a new configuration is mostly based on the potential energy. MC simulation is a powerful tool to investigate time-independent thermodynamics properties, however, does not faithfully describe the time evolution of a system. MD simulation, on the other hand, is appropriate to investigate time-dependent physical phenomenon such as phase transition kinetics, which in this thesis concerns hydrate nucleation. We neglect quantum effects in this study and the MD simulations here are classical. The positions and velocities will be generated after each time step by solving Newton's equations of motion based on the mass of different molecules, the former positions and the inter-molecular potentials. After setting the initial configuration of each molecule and selecting the ensemble (such as the canonical ensemble), the positions and velocities of each molecule will be renewed after each time step and the trajectory can thus be recorded and visualized. Figure 2.1 shows a simplified schematic algorithm of classical MD simulation.

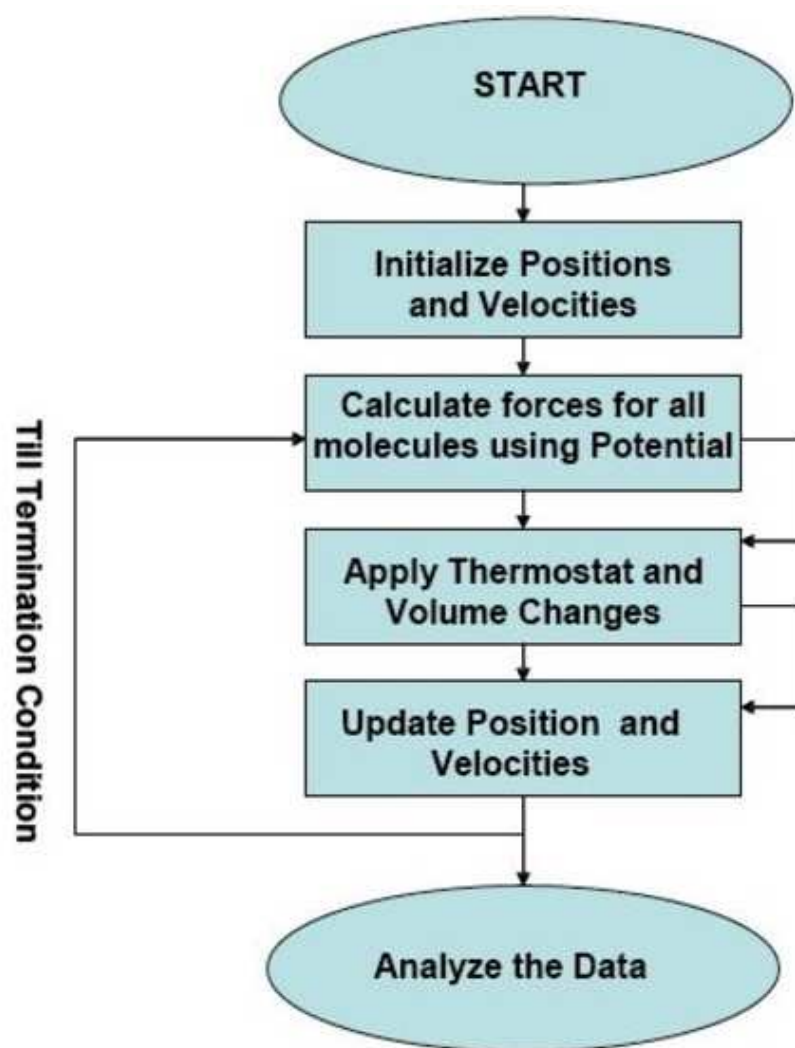


Figure 2.1 A simplified description of the standard classical molecular dynamics simulation algorithm. The flow chart is designed from the description by Frenkel and Smit.⁹⁶

2.3 Simulation Details

The MD simulations were performed using Gromacs 5.1.⁸¹ 2944 TIP4P/Ice⁸² water molecules, 182 CH₄ molecules and 182 C₂H₆ molecules using the OPLS-UA⁸³ force-field model were randomly placed in a cubic box with a length of 4.8 nm. The leap-frog algorithm was used to integrate the equations of motion with full periodic boundary conditions in all

directions. Since the interfacial curvatures have a large effect on the induction time of the simulation due to the Laplace-Young pressure,⁶² it is necessary to keep the initial configuration of the two phase system the same. We performed NVT simulations at 350K for 2 ns at first to make the gas phase assume a cylindrical shape in the box. The configuration of molecules after the NVT simulation was later used in the hydrate nucleation simulation under the NPT ensemble.

The NPT simulations were performed under 255 K and 600,700, and 800 bar pressures respectively. For each condition, 10 simulations were performed with the same initial configuration for 1 microsecond with a time step of 0.002 ps. A Nose-Hoover thermostat with a time constant of 2 ps was used to control the temperature, and the isotropic Parrinello-Rahman barostat was used to keep the pressure with the time constant of 4 ps. The Lorentz-Berthelot combining rules were used for the interactions between the water and CH₄/C₂H₆ molecules. The short-range interactions were truncated at 1 nm and the long-range electrostatics were calculated using the smooth Particle Mesh Ewald (PME) summation algorithm with a Fourier spacing of 0.12 nm. VMD⁸⁴ was used to visualize the trajectories. In order to analyze and visualize the trajectory more efficiently while keep the accuracy and the main information contained in every trajectory, each trajectory was compressed to make each frame represents 0.1 ns length of time. In other words, each trajectory is composed by ten thousand frames. By smoothing the trajectories, the position of each molecule showing on VMD is the averaged position of 10 frames, which means that trajectories were smoothed by averaging 1ns.

Finding the initial hydrate cluster that forms in the simulation box is tricky due to the

very small size of the incipient hydrate nucleus and the disordered motion of molecules in the system. In order to identify the point when the new hydrate phase formed from a disordered two-phase (water and gas) system, the trajectory was run backwards from the end of the simulation till the hydrate cluster became invisible. Later, I found the last 'MCG' structure that disappears, which means, the first 'MCG' structure formed in the system which ultimately grew into hydrate. The induction time is defined as the period before the formation of that first 'hydrate-forming' 'MCG' structure.

2.4 MCG Order Parameter

Unlike the commonly used OPs, such as AOP and F4, which just consider the positions of water molecules (more details can be found in Chapter 4), the Mutually Coordinated Guests (MCG) OP developed by Barnes *et al.*^{58,59} quantifies the appearance and connectivity of molecular clusters composed of guests separated by a water cluster, which is the first two-component OP used for quantifying hydrate nucleation and growth.⁵⁸ MCG-1 was used as an accurate quantitative descriptor for the molecular mechanism for methane hydrate. p_B histogram and equilibrium path sampling methods were used to determine the critical nucleus (MCG-1=16, under 255 K, 500 bar). For simplicity of illustration, a two-dimensional version of the geometry that the algorithm detects is shown in Figure 2.2 and the specific algorithm for identifying MCG monomers and clusters is listed as follows:

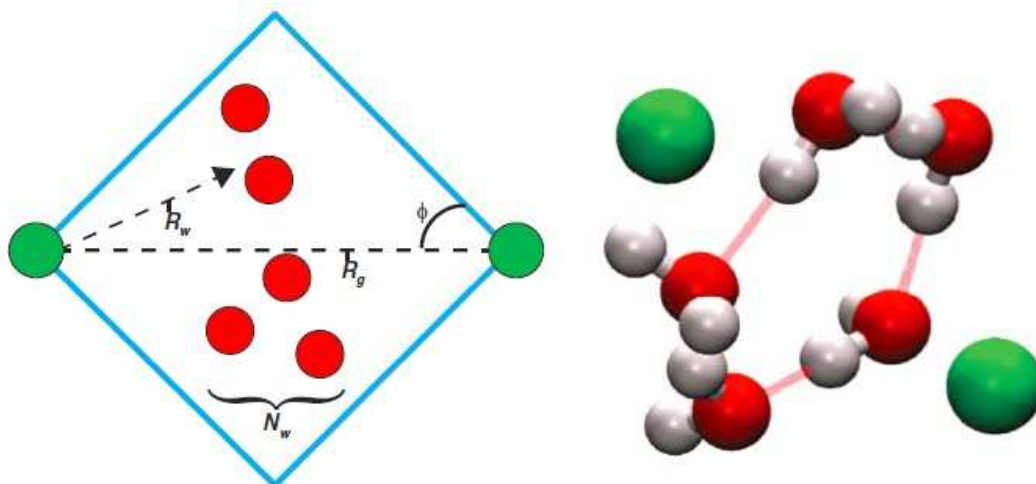


Figure 2.2 Left: Two-dimensional example of one MCG monomer. A given minimum number of water molecules, N_w , must be within a specified angle ϕ of the guest-guest vector. The guests must be within distance R_g^{cut} of each other, and the water molecules must be within distance R_w^{cut} of each guest. Right: A typical structure that the MCG OP seeks to identify. Guests are represented in green and hydrogen bonds are represented in light red lines. (Figure comes from Barnes *et al.*,^{58,59})

1. Searching the guest molecules: for each candidate guest, searching the guest molecules within a given cutoff distance ($R_g^{\text{cut}} = 9 \text{ \AA}$).
2. Searching the host molecules: Set the sweep angles $\phi = 45^\circ$ about the guest-guest vector; water molecules that are within a cutoff distance ($R_w^{\text{cut}} = 6 \text{ \AA}$) from both the candidate guest molecules are considered. We determine if those waters lie within an intersection of cones projected bidirectionally between the candidate guest and its neighbor guest. If there are at least 5 water molecules satisfying these constraints, we successfully identify a 'MCG' monomer.

All the cutoff values were developed based on the structure of hydrate and the radial distribution functions of methane dissolved in water. A schematic representation of the algorithm to identify the MCG clusters for a 2-D non-periodic system is provided in Figure 2.3.

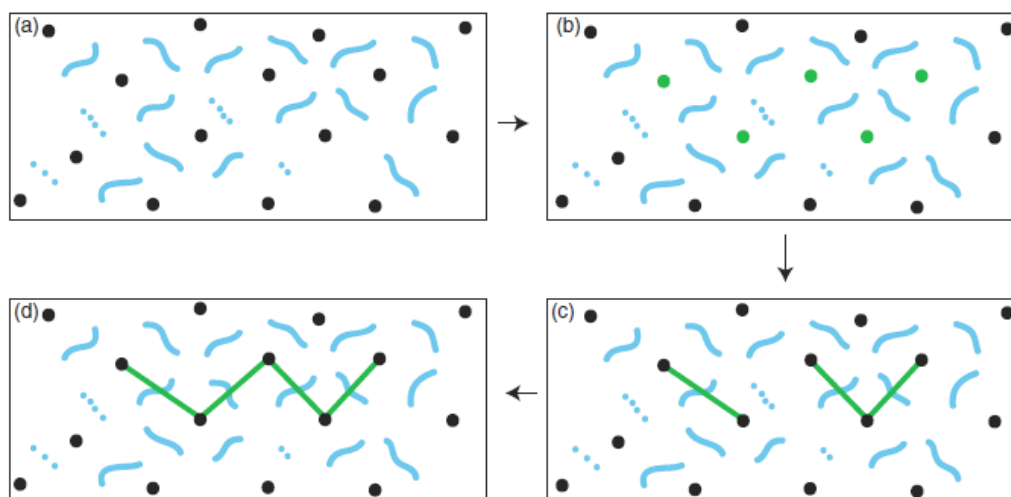


Figure 2.3 Schematic of MCG OP algorithm for a 2-D non-periodic system: (a) The black dots are used to represent the initial guest molecules and the blue lines are used for qualifying clusters while the blue dots for non-qualifying clusters. (b) Mutually Coordinated Guest (MCG) monomers identified (green dots). (c) By searching the MCG monomers, the neighboring monomers are linked into clusters. (d) An Example of clusters that we are going to identify after searching the MCG monomer. (Figure comes from Barnes *et al.*,^{58,59})

In Figure 2.3, initial MCG monomers are identified and then linked into clusters through their neighboring MCG monomers, according to the algorithm introduced above. Graph theory algorithm (e.g. depth-first search for cluster identification) was later used to find the largest MCG cluster. This largest MCG cluster was used to represent the predominant growing hydrate phase. The MCG monomer can be considered as a basic element composing hydrate. By searching for the MCG monomer in hydrate, guest molecules can be detected not only 'in' the hydrate (i.e., enclathrated in the cages), but also on the surface. The results of the composition of hydrate are presented in Chapter 4.

CHAPTER 3

EFFECT OF GAS CONCENTRATION ON THE INDUCTION TIME

3.1 Abstract

In order to understand the pre-nucleation stage of CH₄ and C₂H₆ mixture hydrate, CH₄ and C₂H₆ concentrations are measured under different conditions by analyzing the results from MD simulations. The temperature, interfacial curvature and force field are kept the same while the pressure varies. Higher pressure increases the concentration of dissolved gas molecules (especially C₂H₆) and thus increases the kinetics, such as increasing the nucleation rate, and lowering the time to form incipient hydrate, which will be covered in more detail in Chapter 4. Increasing CH₄ concentration has a clearer trend in terms of decreasing the induction time than for C₂H₆, consistent with the later observation that the first cage formed is usually with CH₄. Moreover, the formation of cages with CH₄ is more kinetically favorable.

3.2 Introduction

A metastable liquid exists under conditions where the thermodynamic phase diagram indicates a more stable phase, with examples such as supercooled and superheated water illustrating their great significance in nature. Another important example is the aqueous solution of hydrophobic gases under high pressure and low temperature, with the liquid being metastable with respect to gas hydrate. As mentioned in the previous chapter, gas hydrate is the main threat to flow assurance in pipelines for the oil and gas industries; as a result, understanding the pre-nucleation stage of hydrate is potentially important to guide strategies

for inhibiting hydrate formation. The thermodynamic globally stable state often cannot be reached immediately (for instance, supercooled water cannot form ice even though the temperature is below the freezing point). As a result, the creation of a phase from the previous phase is characterized by an induction time. The method and the technical details of determining the induction time have been discussed before. Previous studies have shown that temperature, pressure and the interfacial curvature have a great effect on the concentration of CH_4 , and thus influence kinetics such as the nucleation rate.⁶³ To shed new light on metastable $\text{CH}_4/\text{C}_2\text{H}_6$ solutions, the CH_4 and C_2H_6 concentrations under different metastable conditions using MD simulations are examined. In this chapter, the calculation method is first introduced and followed by the results. Our results show that the induction time is shorter in trajectories with a higher CH_4 concentration, consistent with earlier studies.

3.3 Calculation Methods

To calculate the concentrations of CH_4 and C_2H_6 under different metastable conditions, 10 independent simulations were performed under each pressure of interest, and 5 trajectories, 8 trajectories and 10 trajectories formed hydrate under 600 bar, 700 bar, and 800 bar pressure respectively. A schematic of the steps implemented to obtain nucleation trajectories is given in Figure 3.1.

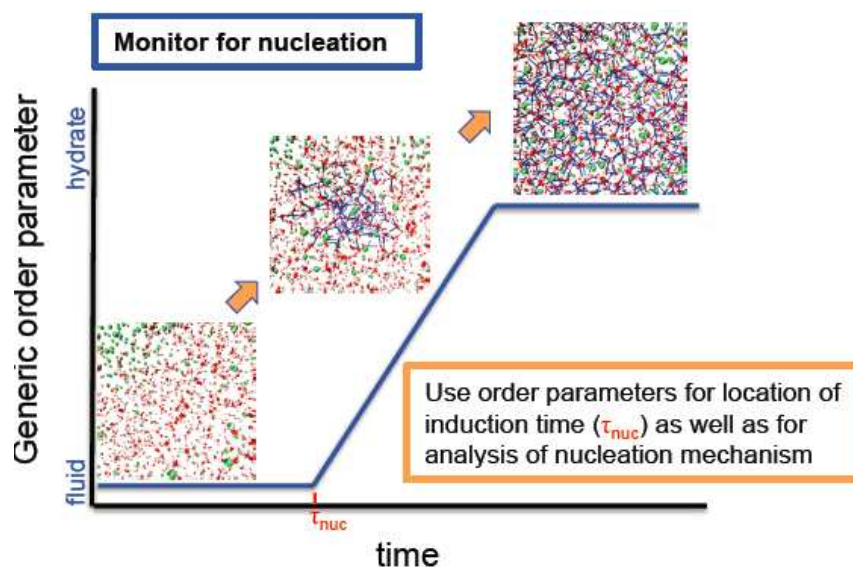


Figure 3.1 Schematic of the steps implemented to obtain nucleation simulations (Figure reproduced from Matt Walsh's Ph.D thesis)

The globally-stable phase cannot be created immediately when entering a new thermodynamic region of the phase diagram, (for instance, the supercooled water cannot form ice immediately although the temperature is below the freezing point), instead, the creation of a new phase is characterized by induction time. In this thesis, we define hydrate induction time as the period from the beginning of the metastable conditions to the moment of formation of the first MCG structure that ultimately grows into non-disappearing hydrate. Although the induction time depends on some factors such as the surface tension between the newly formed phase and the old phase, and the conditions such as the temperature, pressure and aqueous concentration, the length of the induction time is still stochastic.

Order parameters (OPs) are used to monitor and visualize the hydrate nucleation, which is represented on the y-axis in Figure 3.1. Commonly, OPs are numerical functions of the positions of the system's guest and host molecules serving as quantitative indications of different phases. More details on different order parameters will be discussed in the introduction part on Chapter 4. The potential energy of the system can serve as a simple OP

and will drop down when the hydrate forms in the NPT ensemble. Figure 3.2 shows an example of how the potential energy curve varies with simulation time. The potential energy curve is fluctuating but keeping relatively flat overall before hydrate appears. The simulation box remains in two phases while the gas phase keeps a cylindrical shape, as shown in Figure 3.2 (a). The potential energy curve begins to drop down with the appearance of the hydrate. Figure 3.2 (b) and Figure 3.2 (c) show the appearance of the first cage and the first 10 cages respectively. A significant decrease in the potential energy curve can be observed with the increasing size of the newly formed hydrate phase, as shown in the two snapshots Figure 3.2 (d) and (e). Figure 3.3 to Figure 3.5 show the potential energy graphs for all the hydrate formation trajectories under different pressures.

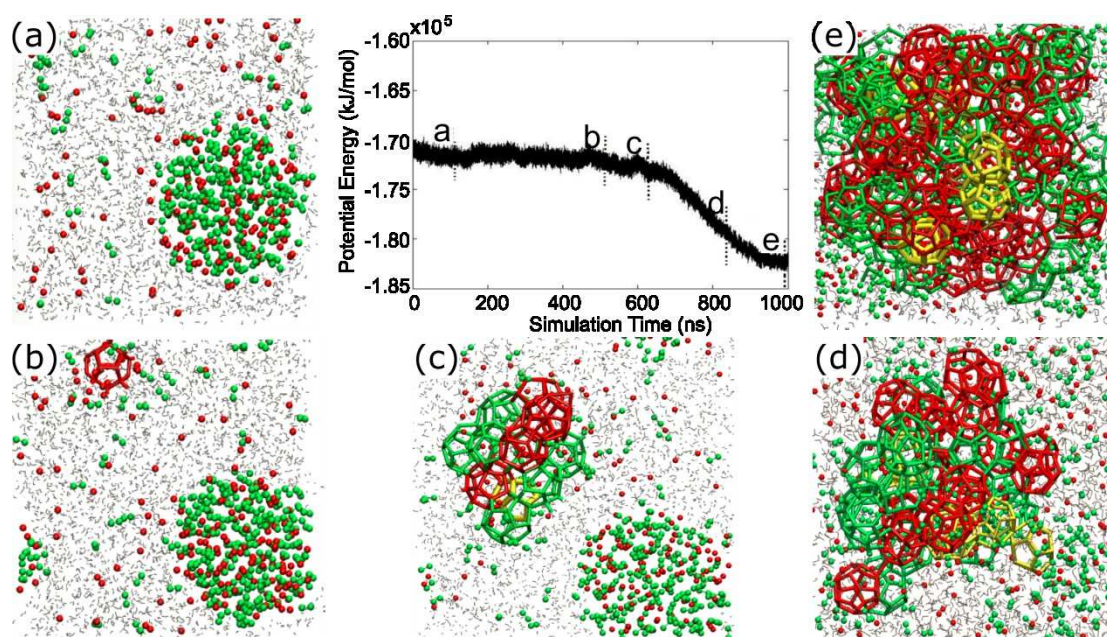


Figure 3.2 An example of the potential energy curve of a hydrate formation trajectory: The snapshots from (a) to (e) show the evolution of the system (red and green dots represent the CH_4 and C_2H_6 molecules respectively. Red lines, green lines and yellow lines represent the cages with CH_4 , C_2H_6 and empty cages. Water molecules are represented by the short gray lines). Before point a, the system was cooled down from the end of the previous NVT simulation and reached a metastable equilibrium condition under an NPT simulation. (a) the initial configuration for the system; (b) the first cage was formed; (c) the first 10 cages were formed. (d) and (e) the hydrate continues to grow through to the end of the simulation.

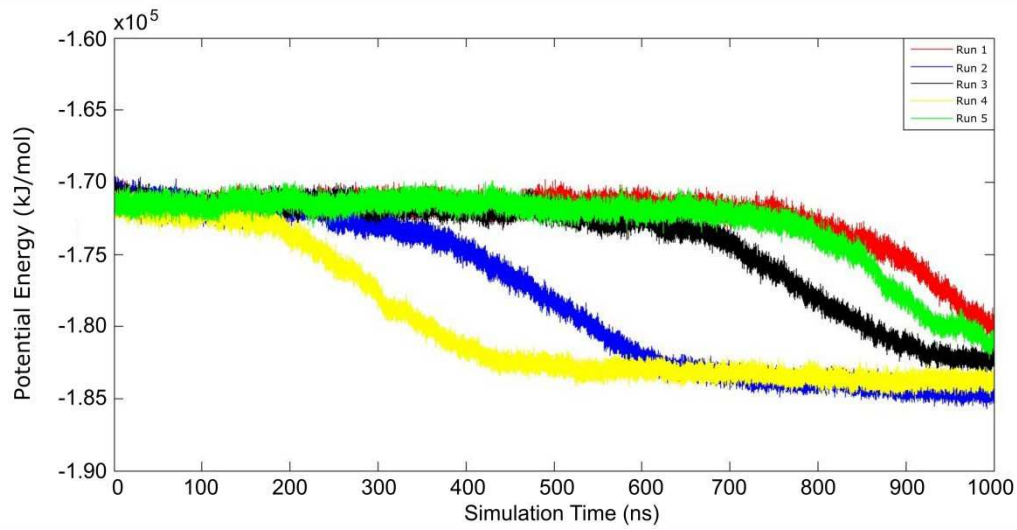


Figure 3.3 Potential energy curve for all the hydrate formation runs under 255 K 600 bar

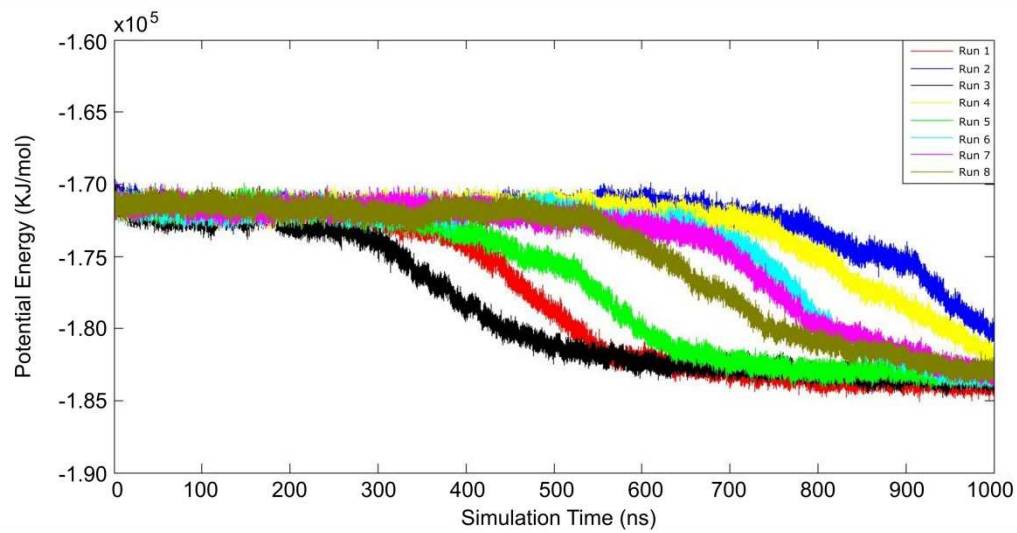


Figure 3.4 Potential energy curve for all the hydrate formation runs under 255 K 700 bar

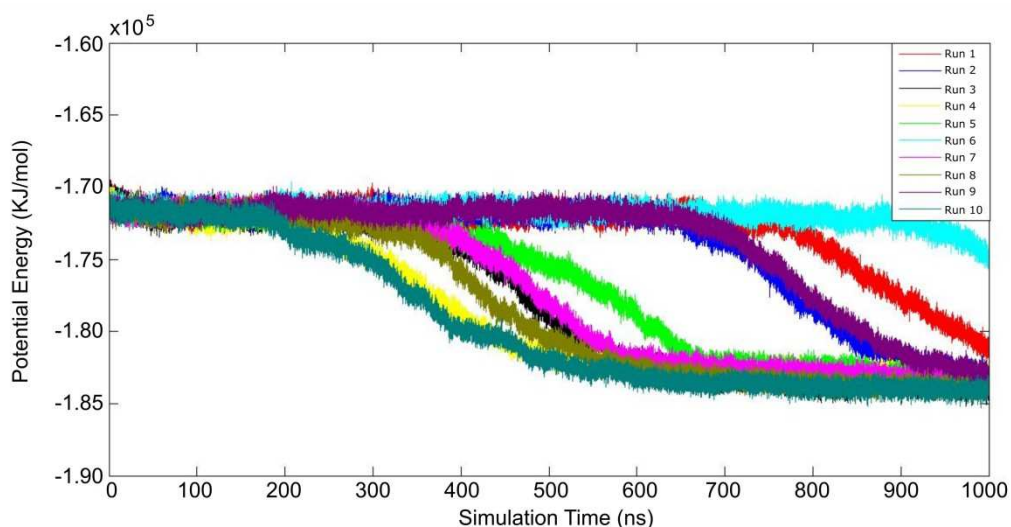


Figure 3.5 Potential energy curve for all the hydrate formation runs under 255 K 800 bar

When the simulations were performed, the cylinder shaped interface between gas mixture and water formed, which can be seen in Figure 3.2. Gas molecules then gradually begin to dissolve into the liquid water. In order to monitor the concentration profile of the system, we divided the z-dimension (which is perpendicular to the interfaces) into 50 parallel slabs with thickness about 0.1 nm. Later, the numbers of CH₄ and C₂H₆ in each slab were calculated for every frame (each frame represents 0.1 ns) within the whole induction period. The results in all the frames were averaged and the typical profiles for the number density of CH₄ and C₂H₆ are shown in Figure 3.6.

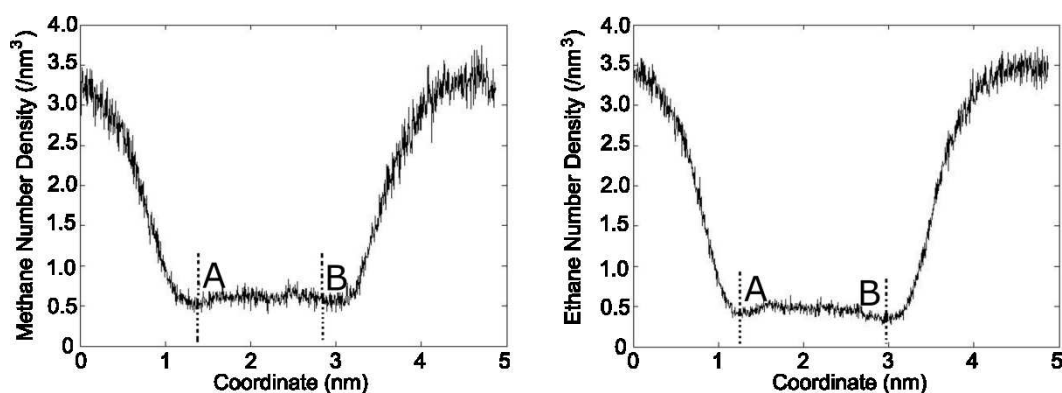


Figure 3.6 Typical profiles across the interface of the system showing the number density of CH₄ (left) and C₂H₆ (right)

From Figure 3.6, the density profiles of CH₄ and C₂H₆ are similar: from the gas phase to solution phase, the density of gas molecules shows a sharp and monotonic decrease into a lower flat region with small fluctuations, as the region indicated as 'AB' that is the liquid phase in the system. All the data within this region were averaged to get the number density of CH₄ and C₂H₆. The results will be shown in the next part.

3.4 Results and Discussions

Previous simulation studies showed that gas concentration in solution could be a key factor increasing the nucleation rate and decreasing the induction time.^{62,85} A recent simulation study based on the gas mixture (CH₄/CO₂) stated that, there was not a clear trend between the induction time and the gas concentration in water,⁶⁸ showing the stochastic nature of hydrate formation. We calculated the concentrations of CH₄ and C₂H₆ in water separately during the whole induction period to compare the difference. The concentration results of CH₄ and C₂H₆ for all the hydrate formation and non hydrate formation runs are listed from Table 3.1 to Table 3.5

Table 3.1 Hydrate formation runs under 255 k, 600 bar

Run #	1	2	3	4	5
CH ₄ mol/L	0.9566	1.2479	1.0282	1.4245	0.9980
C ₂ H ₆ mol/L	0.5718	0.6852	0.8063	0.7056	0.6038
Induction time(ns)	692.2	178.5	415.9	78.2	659.4

Table 3.2 Non hydrate formation runs under 255 k, 600 bar

Run #	6	7	8	9	10
CH ₄ mol/L	1.1210	1.0345	1.0165	1.0396	1.1323
C ₂ H ₆ mol/L	0.6084	0.5345	0.6112	0.5449	0.5863
Induction time(ns)	>1000	>1000	>1000	>1000	>1000

Table 3.3 Hydrate formation runs under 255 k, 700 bar

	1	2	3	4	5	6	7	8
CH ₄ mol/L	0.9407	0.8809	1.1227	1.023	1.0239	1.1893	0.9786	0.9701
C ₂ H ₆ mol/L	0.4870	0.7742	0.8452	0.5114	0.5282	0.7428	0.7073	0.6194
Induction time(ns)	654.5	253.2	204.0	610.1	280.4	507.4	469.8	479.2

Table 3.4 Non hydrate formation runs under 255 k, 700 bar

Run #	9	10
CH ₄ mol/L	1.1611	1.1410
C ₂ H ₆ mol/L	0.6238	0.5751
Induction time(ns)	>1000	>1000

Table 3.5 Hydrate formation runs under 255 k, 800 bar

Run #	1	2	3	4	5
CH ₄ mol/L	1.1714	1.1295	1.2194	1.2842	1.091
C ₂ H ₆ mol/L	0.8365	0.8151	0.6804	0.9133	0.5118
Induction time(ns)	667.0	632.3	258.6	183.3	258.6
Run #	6	7	8	9	10
CH ₄ mol/L	1.1485	1.2531	1.2847	1.0597	1.111
C ₂ H ₆ mol/L	0.5874	0.4862	0.6870	0.683	0.7371
Induction time(ns)	892.9	279.6	251.5	605.4	170.7

The bar plot in Fig.3.7 shows the range of induction times of all the trajectories within the specified concentration range. Comparing Figure 3.7 (a) and (b), we can find trajectories with higher CH₄ concentrations in water have a clearer trend (especially clear in the trajectories of 600 bar) in terms of lowering the induction time than those with C₂H₆, which is constant with the later observation that, the first cage formed in the system is predominately the 5¹² cage with CH₄.

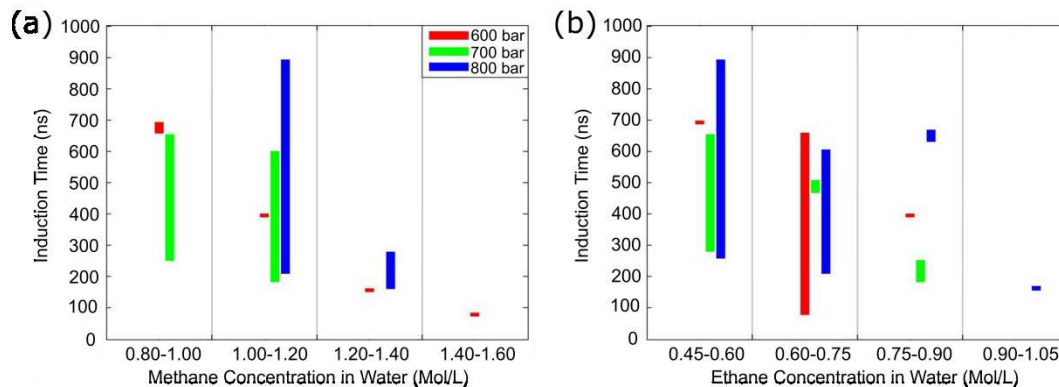


Figure 3.7 Bar plots showing the range of induction time within different ranges of methane (a) or ethane (b) concentration in water.

Not all the trajectories with high CH_4 concentration can ultimately form hydrate in the end. For some non-hydrate forming trajectories, although the CH_4 concentration is high, the C_2H_6 concentration is low, indicating there might be a mutual effect of these two kinds of gas molecules forming the incipient hydrate nucleus. Also, the stochastic nature of hydrate nucleation can also be relevant. However, note that I calculated the aqueous gas concentration in the liquid phase of the whole box, which is not the local concentration. For some non-nucleation trajectories, there might be a lack of a local high concentration place.

3.5 Conclusions

30 microsecond MD simulations were performed to study the hydrate nucleation of CH_4 and C_2H_6 mixture and the investigation of the concentrations of different guest molecules is crucial in the pre-nucleation stage. By analyzing the hydrate formation trajectories, the concentration of different guest molecules in water has been determined. The interfacial curvature was kept the same for all the simulations to avoid the effects from the interface on

the concentrations. After comparing all these results, we found higher CH_4 concentrations in water decrease the induction time, consistent with the later observation that the first cage formed is usually with CH_4 . By contrast, no strong effect of C_2H_6 concentration on induction time was observed. The stochastic nature of hydrate nucleation can be observed from all the results, wherein some trajectories do not form hydrate despite a relatively high guest concentration. Finally, high aqueous CH_4 concentration may not be the only relevant factor for the short induction time, indicating there might be a mutual effect of both the guest molecules. This question remains open and requires future work.

CHAPTER 4

THE INITIAL CAGES AND THE CAGE STABILITY

4.1 Abstract

In this chapter, the incipient hydrate structure was analyzed by analyzing the first ten cages formed in the system. Our results show that the majority of the incipient cages are 5^{12} cages with CH_4 . The formation of cages with CH_4 is more kinetically favorable (independent from the concentration in the hydrate phase), especially the early formation of 5^{12} cages with CH_4 can provide a hydrate-like cage structure for C_2H_6 , which has otherwise a larger difficulty to form hydrate. In addition, increasing CH_4 concentration decreases the induction time, which is the main conclusion made in the previous chapter, consistent with the observation that the first cage formed is usually the 5^{12} cage with CH_4 . Higher pressure increases the nucleation rate, the cage diversity and C_2H_6 involvement. Moreover, the stability of the cages with CH_4 increases with pressure, while the opposite trend can be found for cages with C_2H_6 .

4.2 Introduction

Gas hydrates have a crystalline structure composed of different cages formed by hydrogen bonded water molecules that trap guest molecules. The three common clathrate hydrate structures are structure I (sI), structure II (sII) and structure H (sH). Both pure CH_4 and C_2H_6 can form sI hydrate. The sI unit cell is composed of two pentagonal dodecahedron (5^{12}) cages and six tetradecahedron ($5^{12}6^2$) cages.

Order parameters (OPs) are numerical functions of the positions of the system's guest and host molecules serving as quantitative indications of different phases. Bi *et al.* developed the H-COP order parameter, which used the number of water molecules in the largest cluster to quantify hydrate nucleation and growth.⁵⁵ The angular order parameter (AOP) and four-body structural order parameter (F₄), are the most commonly used OPs in many publications.^{40,86-89} The AOP defined as follows describes the local angular ordering of water molecules

$$AOP = \left\langle \sum [(|\cos \theta| \cos \theta + \cos^2(109.47^\circ))]^2 \right\rangle \quad (1)$$

where θ is the inclusion angle for the oxygen atom of the water molecule of interest and any two oxygen atoms of neighboring water molecules. The summation runs over all possible θ values of water molecules within a radius of 0.35 nm from the central oxygen atom of interest. The value of AOP is about 0.8 for liquid water, 0 for ice and 0.1 for hydrate.

The F₄ OP measures the planarity of water pairs as follows

$$F4 = \langle \cos(3\phi) \rangle \quad (2)$$

where ϕ is the dihedral angle H¹-O¹...O²-H² formed by two neighboring water molecules within 0.35 nm, with H¹ and H² being the farthest hydrogen atoms on each of the water molecules. Typical F₄ values are 0.1 for liquid water, 0.89 for sI hydrate, 0.96 for sII hydrate and -0.5 for ice.

Although AOP and F₄ can be two convenient OPs to distinguish hydrate from water and ice, these two OPs do not account for guest molecules. Barnes *et al.* developed a new OP combining both guest and host molecules called the mutually coordinated guests (MCG) OP.⁵⁸

⁵⁹ The details and the algorithm have been introduced above. In this thesis, MCG is the OP

used to identify hydrate nucleation and growth. The largest MCG cluster is used to represent the hydrate phase.

Cage preferences are different for CH₄ and C₂H₆ molecules in hydrate due to their different sizes. Compared with the 5¹² cage, the 4¹5¹⁰6² cage with an oblong shape fits the size of a C₂H₆ molecule. With only 22 water molecules, the formation of the 4¹5¹⁰6² cage is kinetically favorable and is the first cage formed. In contrast to the pure CH₄ system, where the 5¹² cage is the most prevalent and initiates hydrate formation,^{54,62} the 4¹5¹⁰6² cage is most prevalent in the pure C₂H₆ system, indicating the important role of this metastable cage. In the mixture system, the formation of cages with CH₄ is more kinetically favorable, especially the small pentagonal dodecahedron (5¹²) cages. The formation of the cages with CH₄ can provide hydrate-like cage structure for C₂H₆, and can thus form hydrate under a relatively lower driving force.

A cooperative adsorption mechanism has been reported in many studies and the details have been introduced before. In a nutshell, this mechanism provides positive feedback for ordering of guest molecules and host molecules: at the beginning, the planar water faces connected by hydrogen bonds absorb guest molecules, due to the hydrophobic property of methane, water molecules will form cage-like rearrangement around these adsorbed guests, which in turn protect the incipient hydrate cluster from dissociation and favor the further growth of hydrate. This process eventually leads to the formation of a full cage which provides more guest adsorption sites and promote the hydrate formation. This process eventually leads to the formation of a full cage which provides more guest adsorption sites and promotes hydrate formation. Based on this mechanism, one expects that a cage with a

higher stability should have favor the growth of a hydrate cluster, especially when the hydrate is newly formed since a cage with high integrity can provide more faces to absorb guest molecules.

4.3 The Incipient Cages and Pressure Effects

This study focused on the early stage behavior of hydrate nucleation and studied the first 10 cages that formed in the system. My observations suggest that if the size of the hydrate cluster can successfully form 10 cages, it is apparently larger than the critical nucleus size under these conditions, as hydrate then grows spontaneously. Two water molecules are considered connected if their two oxygen atoms are within 0.35 nm and the cage identification geometry is the same as proposed by Jacobson *et al.*⁹⁰ The cage transformation and destruction-recovery phenomenon is very common,⁶³ since parts of the incipient cages are exposed to the rapidly fluctuating water phase. Not all the initial cages can survive to the end, but at the early stages of hydrate formation, a completed cage is observed to be very effective in terms of attracting more gas molecules, and prolonging the lifetime of the faces of unconstrained cages.^{51,54} As a result, I counted a cage as an 'initial cage' in this study if that cage can exist for longer than 1 ns.

Figure 4.1 shows the fraction of different types of incipient cages (the first 10 cages) under different pressures. The majority of the initial cages are 5¹² cages with CH₄, and this type of cage is always the first one that forms in the system (with only one exception under 800 bar, where the first cage is a 4¹⁵6² cage with C₂H₆, which will be discussed later). This

observation is in accord with the experimental study by Schick *et al.*,^{77,78} suggesting an important role for the 5^{12} cages with CH_4 to initialize hydrate formation. The fraction of cages with C_2H_6 increases with pressure, especially the $4^15^{10}6^2$ cage. Higher pressure can also increase the diversity of cages, as we can see from the red bars in Figure 4.1, and is similar to the effect of a high degree of subcooling. Higher order crystalline structures can be found under lower degrees of subcooling⁹¹ or in constant energy system.^{64,65}

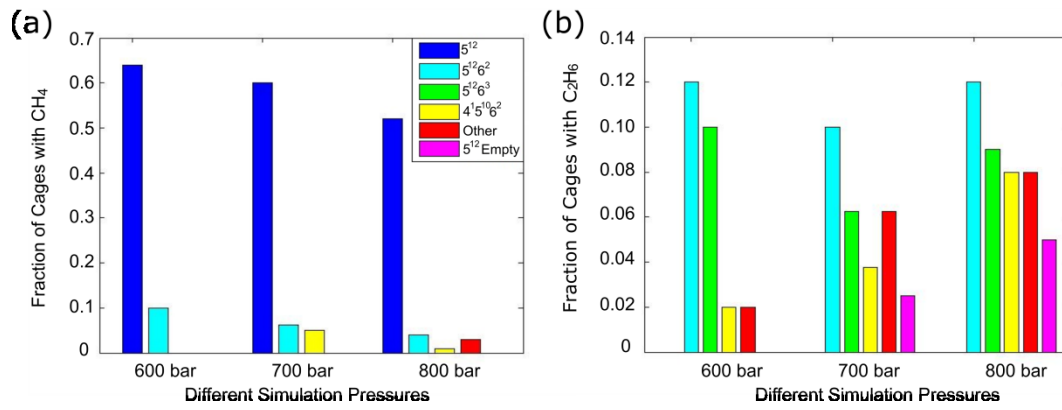


Figure 4.1 Fraction of different initial cages with (a) CH_4 and (b) C_2H_6 under different pressures (the first 10 cages were counted in each trajectory). Other cages with CH_4 represent uncommon ones: $4^25^86^3$, $4^15^{10}6^3$; for cages containing C_2H_6 , the uncommon cages are $5^{12}6^4$, $4^15^{10}6^3$, $4^15^{10}6^4$, and 5^{12} .

The nucleation rate⁹² was calculated using equation 3:

$$Rate = \frac{N_R}{(\sum_i^{N_R} \tau_i + \sum_j^{N_{NR}} \tau_j) * V_{liq}} \quad (3)$$

where N_R is the number of reactive (nucleating) trajectories, N_{NR} is the number of non-reactive trajectories, τ_i is the induction time for the i th trajectory; τ_j is the total simulation time (1000 ns) for the j th non-nucleating trajectory; V_{liq} is the volume of aqueous phase at the conditions of interest. Figure 4.2 illustrates the effect of pressure on the hydrate nucleation kinetics. With increasing pressure, the time to form the first 10 cages, as well as the time between the first cage and the first cage with C_2H_6 , decreases while the nucleation

rate increases. This decrease in time and increase in variety is a behavior characteristic of faster quenching of a phase transition.

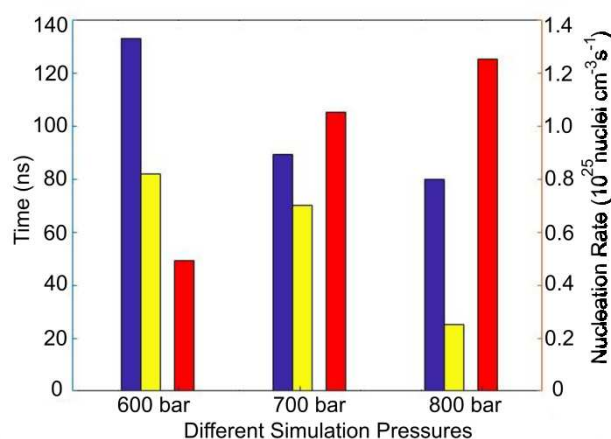


Figure 4.2 The average time (averaging over all hydrate-forming runs) to build the first 10 cages (blue bars), between the first cage and the first cage with C₂H₆ (yellow bars) and the nucleation rate (red bars, right y-axis) under different pressures.

4.4 Composition of the Incipient Hydrate

In order to identify gas hydrate in the simulation box, the system was searched for 'MCG' monomer as a building block of hydrate. A hydrate cluster can be formed by many 'MCG' monomers. After that, the largest cluster was identified. I focused on the incipient period of hydrate formation and counted 30 ns before the formation of the first cage and 100 ns after, since 30 ns is about the time between the appearance of the first 'MCG' monomer that ultimately grows into a completed cage, and 100 ns is about the time to form the first 10 cages. Figure 4.3 shows three typical examples of the composition of CH₄ and C₂H₆ in the largest MCG cluster during the initial period: more CH₄ than C₂H₆; CH₄ is nearly the same as C₂H₆ or lower than C₂H₆ at the very beginning. Moreover, from the insets, we can see CH₄

outnumber C_2H_6 in the hydrate phase especially during the later growth period of hydrate.

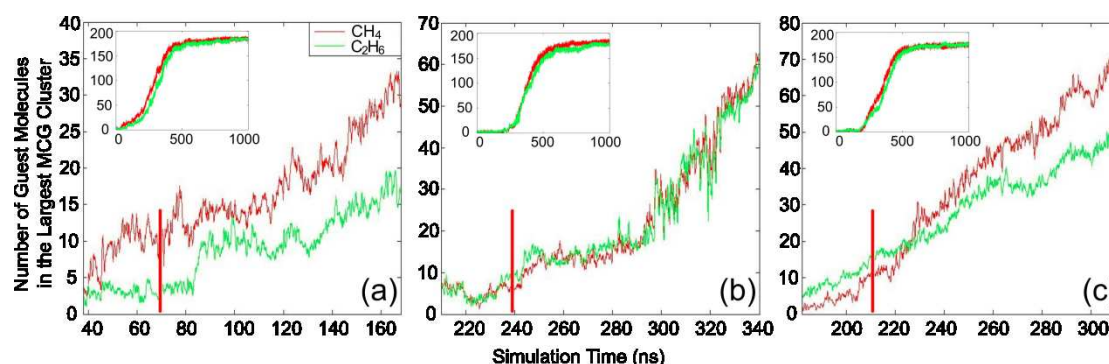


Figure 4.3 The number of CH_4 and C_2H_6 molecules in the largest MCG cluster in the hydrate phase at the initial stage of hydrate formation. The vertical red line indicates the point when the first cage was formed. 30 ns was counted before the red line and 100 ns was counted after. Case (a), CH_4 outnumber C_2H_6 ; Case (b), the number of CH_4 is nearly the same as the number of C_2H_6 ; Case (c), C_2H_6 outnumber CH_4 at the very beginning; the insets illustrate the number of CH_4 and C_2H_6 in the largest MCG cluster for the entire simulation time.

The first two cases are observed in almost all the different trajectories under different pressures, while the third case only occurred once under 800 bar. There C_2H_6 outnumbered CH_4 in the largest MCG cluster before the formation of the first cage, and a $4^15^{10}6^2$ cage with C_2H_6 initialized the hydrate formation instead of a 5^{12} cage with CH_4 , as was the case in all the other trajectories. Typically, the fraction of the incipient cages with C_2H_6 in case (b) is higher than the fraction in case (a).

Although there is a difference in the concentration of CH_4 and C_2H_6 in the incipient hydrate phase in all the three cases, more than half of the initial 10 cages are the ones with CH_4 in every trajectory. This suggests that the formation of cages with CH_4 (especially the 5^{12} cage), which is independent of the concentration in the incipient new hydrate phase, is more kinetically favorable. CH_4 outnumber C_2H_6 in the hydrate cluster during the hydrate growth period, and in the end is caught up by C_2H_6 because of the depletion of CH_4 in the gas phase.

4.6 Cage Stability

Pressure can increase C_2H_6 involvement, as shown in Figure 4.1: the fraction of cages with C_2H_6 increases under higher pressure. It is important to consider the number of completed cages or partial cages in contact (sharing faces) with the first cage with C_2H_6 . Fewer completed cages and partial cages surround the first cage with C_2H_6 under the higher pressure, as shown in Figure 4.4. Figure 4.4 (a) is an example snapshot showing the surrounding structure under lower pressure while (b) is a snapshot from a trajectory under higher pressure. Two examples of the formation process of the first cage with C_2H_6 under lower pressure and higher pressure are shown in Figure 4.5 and Figure 4.6 (snapshots from Movie 1 and Movie 2) respectively.

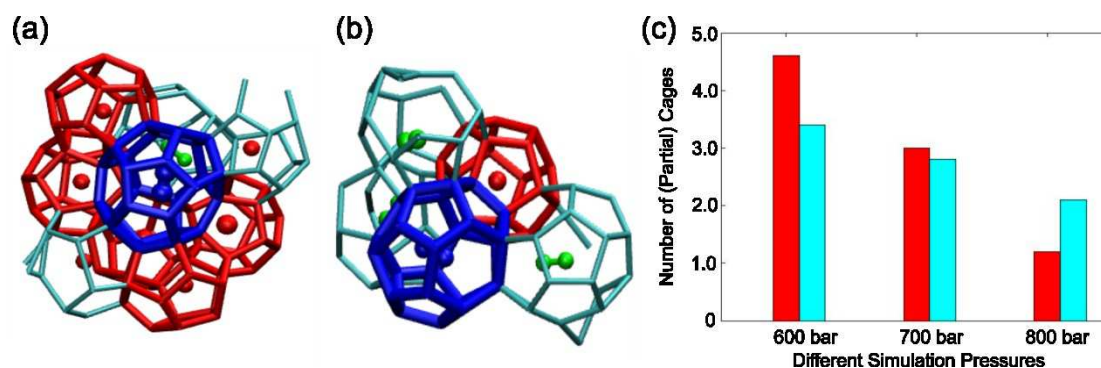


Figure 4.4 Two typical snapshots show the moment when the first cage with C_2H_6 appears under (a) lower pressure and (b) higher pressure. The thick blue cage represents the first cage with C_2H_6 ; red and cyan lines represent the completed cages with CH_4 and partial cages respectively. Red and green balls represent CH_4 and C_2H_6 . The number (averaged over all the trajectories) of completed cages (red bars) and partial cages (cyan bars) sharing faces with the first cage with C_2H_6 that formed are plotted for different pressure. Here, we define partial cage as one that has at least 6 faces.

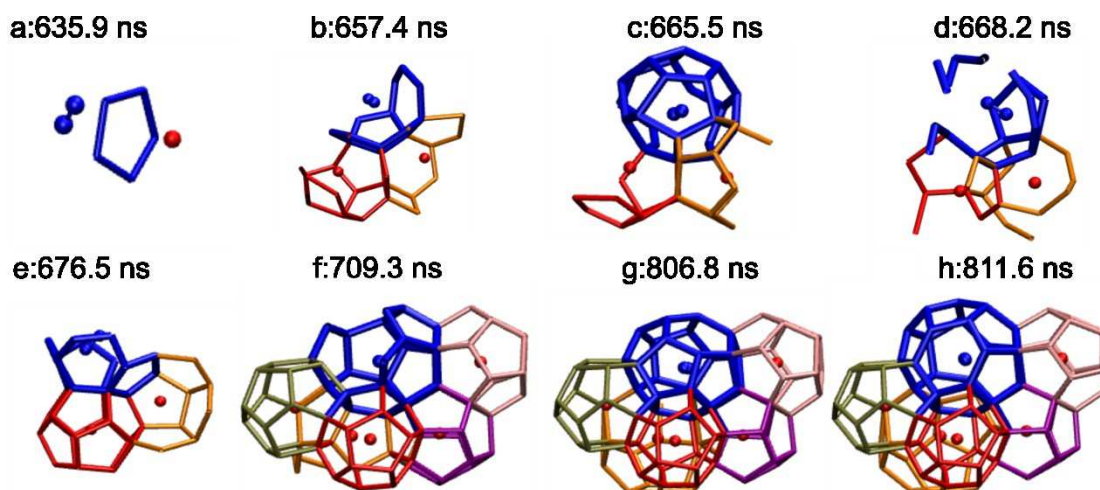


Figure 4.5 The formation process of a cage with C_2H_6 from a trajectory at 700 bar (we highlight the blue C_2H_6 molecule). (a), the target blue C_2H_6 molecule and a red CH_4 molecule absorbed on either side of a single water ring composed of 5 water molecules. (b), the target blue molecule starts to form a cage near two partial cages with CH_4 . (c) to (d), the blue C_2H_6 molecule almost forms a cage but the cage is not stable, it falls apart immediately. (e) to (f), more 5^{12} cages with CH_4 which are kinetically favorable, form around the C_2H_6 molecule. (g) to (h), the blue C_2H_6 forms a $5^{12}6^2$ cage and later, transforms into a $5^{12}6^3$ cage.

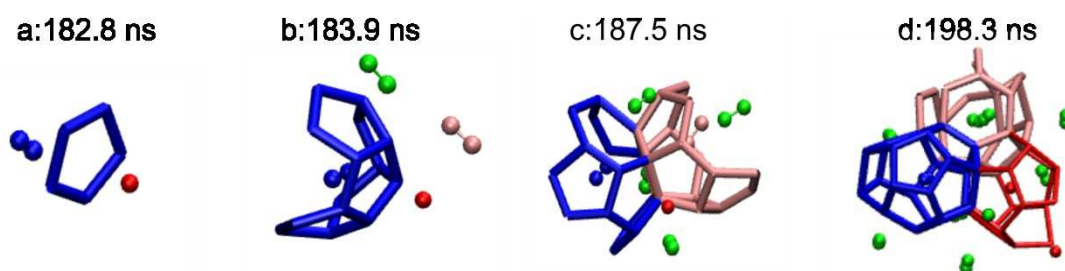


Figure 4.6 The formation of a cage with C_2H_6 corresponding to Fig.4.3 (c), which occurred under high pressure (800 bar). (a), a blue target C_2H_6 molecule and a red CH_4 molecule absorb on either side of a ring composed of 5 water molecules. (b), more water and guest molecules come together around the blue target C_2H_6 molecule. (c), the blue and the pink C_2H_6 molecules begin to form the bowl-like partial cages. (d), the blue C_2H_6 molecule formed a $4^{15}106^2$ cage, which is the first cage that formed in the system.

From snapshot (c) in Figure 4.5, the C_2H_6 molecule almost formed a cage, but it was not stable enough under low pressure without enough support from the surrounding cage-like structures, and so fell apart rapidly. The target blue C_2H_6 molecule then traveled into a saddle part of the other partial cages. The role of the cage-like structure formed by CH_4 cages is

similar to a nucleation site and template to provide a place for C_2H_6 molecules to inhabit. Sharing faces with some completed or partial cages with CH_4 , the C_2H_6 molecule successfully formed a cage in the end, thanks to the 'support' from the formation of the kinetically favored cages with CH_4 .

Figure 4.6 illustrates another, more exceptional, example under high pressure of the formation process of a cage with C_2H_6 and case (c) in Figure 4.3 illustrates the concentration of CH_4 and C_2H_6 in the hydrate for this same trajectory. The first cage formed is a $4^15^{10}6^2$ cage with C_2H_6 , without sharing many faces from the cages or partial cages formed by CH_4 , as was needed at lower pressure as seen in Figure 4.5. Instead, here the formation of the $4^15^{10}6^2$ cage with C_2H_6 occurs more independently. The independent formation of a $4^15^{10}6^2$ cage with C_2H_6 is consistent with the observation that in the nucleation of pure C_2H_6 hydrate system, the $4^15^{10}6^2$ cage also forms first.

Usually a cage can be stable (with no transformation or destruction) for several ns after it is formed. Cage transformation and destruction-reformation are common at the early stages of hydration formation. Exposed to the highly fluctuating nature of hydrogen bonding in water, cages on the surface of the incipient hydrate nucleus are not always stable. An example can be seen in a third trajectory, where both of these two cages underwent destruction after they were formed. However, more water molecules in one cage are involved in the fluctuation than another one, since a 'cage appearance' can still be observed for the latter cage which means it can still keep a higher integrity. On the contrary, the first cage has less integrity. Based on the maximum internal diameter of different types of cages from Table 4.1, we tracked the number of water molecules within a certain type of cage radius of the gas

molecule after a cage was formed. Figure 4.7 (a) provides an unbiased view from Movie 3, while Figure 4.7 (b) from Movie 4 provides an example of the water fluctuation when cage transformation occurs.

Table 4.1 Cage diameter of the seven most dominated cages

Cage Type	Max Internal Diameter (nm)	Cavity Diameter (nm)
5^{12}	0.85	0.57
$4^1 5^{10} 6^2$	0.90	0.64
$5^{12} 6^2$	0.95	0.67
$5^{12} 6^3$	0.99	0.70
$5^{12} 6^4$	1.00	0.72
$4^1 5^{10} 6^3$	0.98	0.70
$4^1 5^{10} 6^4$	0.99	0.71

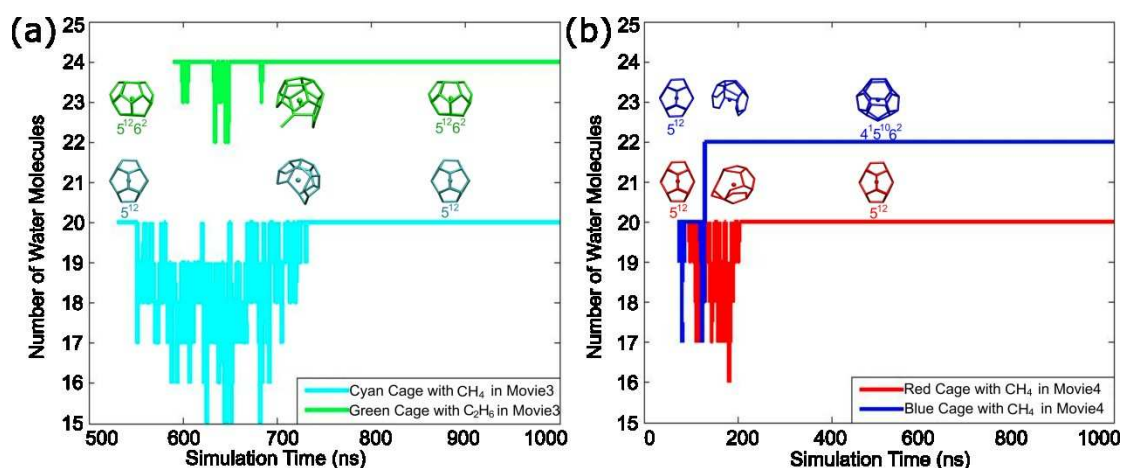


Figure 4.7 Cages fluctuate in the number of water molecules after formation. Panels (a) and (b) come from Movie 3 and Movie 4 respectively.

The cage transformation and destruction-reformation can be detected when the number

of water molecules changes. Similar to the standard deviation which reflects the amount of variation, we used equation (1) to calculate the fluctuation of water movement. This phenomenon happens mostly at the beginning when the newly formed cages are still on the surface, tracking the fate of cages for 150 ns after they formed is long enough to include the period when cages undergo the majority of the transformation or destruction and reformation. In equation (1), n is the number of water molecules within the cutoff distance. In the case of a cage transformation, N_{type1} and N_{type2} are the number of water molecules for the first and second type of cage (for instance, 20 for 5^{12}); t_1 is the time counted from when the first type of cage was formed until the middle of the period from the breaking of the first type of cage to the formation of the second type of cage. t_2 is counted from the end point of t_1 to the middle of the period between the breaking of the second type of cage and the formation of the third type of cage. Figure 4.8 (a) shows the result of all the fluctuation values (F Value) for all the cages under different pressures. Moreover, the "F value" for different kinds of cages were also calculated (here, if there is cage transformation, we only use the first part of equation 1) which is illustrated in Figure 4.8 (b). For the cages containing CH_4 , we calculated two most common types: 5^{12} and $5^{12}6^2$; for the cages with C_2H_6 , three most common types were calculated: $4^15^{10}6^2$, $5^{12}6^2$ and $5^{12}6^3$.

$$F_value = \sqrt{\frac{\sum (n - N_{type1})^2}{t_1}} + \sqrt{\frac{\sum (n - N_{type2})^2}{t_2}} + \dots \quad (4)$$

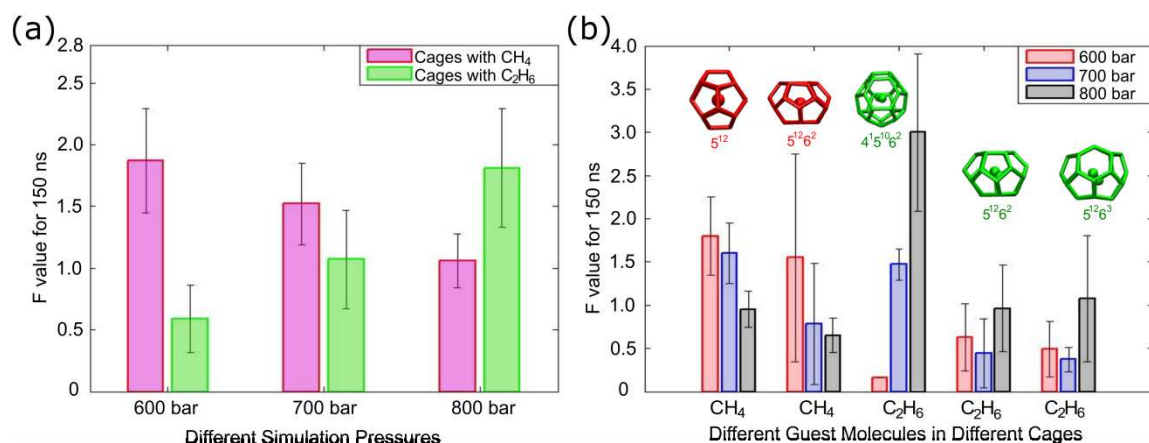


Figure 4.8 The F _value for all the cages under different pressures (a) and different cages with different guest molecules (b). The error bars show the 95% confidence interval of the mean.

The degree of fluctuations in the number of water molecules in the cages with CH₄ decreases with pressure. Smaller error bars can be found on the 5¹² cages showing that the water fluctuation has a stronger correlation with pressure than for 5¹²6² cages. The large error bars on the 5¹²6² cage with CH₄ indicates a great variability in terms of stability: some cages are very stable while some are not. The reason for the decreasing fluctuation of water movement for the cages with CH₄ can be explained from the kinetics results in Figure 4.2: The cage transformation and destruction-recovery phenomenon happens frequently with more water molecules participating on the growing hydrate surface. Higher pressure decreases the time for the surface of a newly formed cage with CH₄ to be exposed. Surrounded by cages and guest molecules, the cage with CH₄ will be more stable with less fluctuation.

In contrast, water fluctuations for the cages with C₂H₆ increases with pressure, especially for 4¹5¹⁰6² cages. The first cage with C₂H₆ appears sooner with less face sharing with surroundings cages or partial cages under high pressure. As a result, more faces of the cage are exposed to the water environment. The pressures in this study (600, 700, 800 bar)

are higher than that used in the pure CH₄ hydrate simulation system (500bar), but much lower than the pure C₂H₆ system simulation study (1300bar).⁷³ We also performed 10 pure C₂H₆ simulations with the same number of guest/host molecules with the same initial configuration of gas phase under 255K and 800 bar, but none formed hydrate. In other words, the driving force is high enough to make water and methane into clathrate, but not enough for C₂H₆. If the driving force is not large enough to crystallize a compound, an additive that is easier to be crystallized is helpful by providing the early hydrate-like structure as the template for the other compound with a greater difficulty to crystallize.

Trajectories at 800 bar pressure behave more similarly to the pure C₂H₆ system because of the higher C₂H₆ involvement in the incipient hydrate and the locally high C₂H₆ concentration can even initiate hydrate formation. Larger cages with more water molecules as well as more hydrogen bonding, therefore, have higher stabilization energies than small cages.⁶⁷ As a result, smaller cages with fewer water molecules tend to form first, consistent with the observation that CH₄ tends to form 5¹² cage, while the metastable 4¹5¹⁰6² cage, which is the second smallest cage with an oblong shape and larger size than the 5¹² cage, fits the size of C₂H₆. Also, the 4¹5¹⁰6² cage is kinetically favorable and suitable to accommodate linear molecules such as C₂H₆ and CO₂.^{62,92} The formation of 4¹5¹⁰6² cages with C₂H₆ occurs more independently from surrounding structure under higher pressure. From the previous study, we can see that the 4¹5¹⁰6² cage usually forms first in the pure C₂H₆ system. With more faces exposed in the water phase, the 4¹5¹⁰6² cage with C₂H₆ has a higher degree of fluctuation. The high fraction of the 4¹5¹⁰6² cages can be attributed to an important factor for larger fluctuations for the cages with C₂H₆.

Previous studies based on potential of mean force (PMF) calculations show that there is a strong attractive interaction between a completed cage and guest molecules.^{51,92} The adsorbed guest molecules, can in turn, make the water molecules nearby more ordered due to the "hydrophobic" interaction. This positive feedback is important in hydrate growth, especially at the early stage when the newly formed solid phase has a strong tendency to dissolve back to liquid. A study on the growth of THF hydrate suggested that the open small cages that THF molecules prefer on the hydrate surface, explains why THF inhibits crystal growth.⁸⁴ From Movie 1 and Movie 2, the crystal did not grow toward the direction where the faces of a cage are still fluctuating. Thus, it is reasonable to deduce, a cage should have a more significant effect in terms of stabilizing the initial hydrate nucleus if it can be stable for a longer time and cages with C₂H₆ stabilize the early stage nucleus under low pressure, while cages with CH₄ have this role under high pressure.

4.7 Conclusions

In qualitative accord with experimental studies, the 5¹² cage with CH₄ initiates hydrate formation, which is also consistent with the results from examining the effects of guest concentration: trajectories with higher CH₄ concentrations in water have a stronger effect lowering the induction time. The majority of the incipient cages are the ones with CH₄, especially the 5¹² cages. Independent from the concentration in the hydrate phase, the formation of cages with CH₄ is more kinetically favorable. The effect of pressure was also studied: higher pressure increases the kinetics, such as increasing the nucleation rate while decreasing the time to build the first 10 cages of the incipient hydrate.

The hydrate phase was identified by searching for the 'MCG' monomer, which can be considered as a building block of hydrate. The composition of hydrate at the incipient phase is stochastic, but with three cases observed. CH₄ outnumbered C₂H₆ in the hydrate growth period. When observing the details of how a C₂H₆ forms a cage, we find under high pressure, the formation of cages with C₂H₆ shows less dependence on the surrounding solid structures, while under low pressure, more surrounding cage-like structure can be found around the first cage with C₂H₆.

Cages are typically not initially stable after they are formed. Previous studies have showed that the cage-transformation and destruction phenomenon happens frequently. We developed an 'F value' statistic to measure the stability of cages, similar to the standard deviation. Cages with CH₄ will be protected by more cage-like structure formed by water under high pressure, but with more parts of the cages with C₂H₆ exposed in the water phase. Thus, the stability of cages with CH₄ increases, while cages with C₂H₆ decrease with pressure. Under high pressure, the fraction of 4¹5¹⁰6² cages with C₂H₆ increases with decreasing stability. The reason for the low stability or the high water fluctuation for the cage is because more parts of the cage are exposed to water not covered by hydrate, which is consistent with the observations from the C₂H₆ hydrate system where the 4¹5¹⁰6² cage is most prevalent and can form most independently (forms first). Based on the cooperative adsorption mechanism of hydrate formation, cages with higher stability should be more helpful to stabilize incipient hydrate cluster. As a result, I hypothesize that cages with C₂H₆ are more stable and stabilize the hydrate cluster under lower pressures, while cages with CH₄ have this role under higher pressures.

CHAPTER 5

CONCLUSION AND FUTURE WORK

Microseconds MD simulations were performed to study the nucleation of CH₄ and C₂H₆ mixture hydrate. From our results, higher pressure increased the kinetics, the cage diversity and C₂H₆ involvement, similar to the effects of higher subcooling. Higher aqueous CH₄ concentration has a more significant trend lowering the induction time than for C₂H₆, consistent with the fact that the first cage formed in the system is a 5¹² cage with CH₄. In accord with hypotheses generated by experiments, the role of the 5¹² cage with CH₄ is to initialize the hydrate formation. However, it should be cautioned that the experiments probe the much later growth phase in the formation of hydrate, compared to nucleation. The formation of cages with CH₄, especially 5¹² small cages, is kinetically favorable and is also independent from the guest composition in the hydrate phase. A higher driving force is needed for C₂H₆ to form hydrate, but the early formation of kinetically favored cages with CH₄ can provide hydrate-like cage structure for C₂H₆ to form hydrate with less difficulty, whose role is more or less similar to nucleation sites from a substrate. Based on the important role of a completed cage and the cooperative adsorption mechanism of hydrate formation, I propose that cages with lower fluctuations can stabilize the incipient hydrate cluster. Cages with C₂H₆ and CH₄ are more stable under low and high pressure respectively, as measured by fluctuation degree, and thus have a stronger effect to stabilize the newly formed hydrate.

Many differences can be concluded between the formation of hydrate from the pure CH₄ and C₂H₆ systems. First, we need higher driving force for C₂H₆ and water to form hydrate than CH₄ from the simulation study. The smallest 5¹² cage with twenty water molecules and

the highest symmetry among all the cages, tends to form first in the simulation box, in part due to having the lowest entropy penalty. Furthermore, larger cages with more water molecules and hydrogen bonds are more difficult to form kinetically, and possibly thermodynamically. Due to the larger size, C_2H_6 cannot fit the smallest 5^{12} cage, and instead prefers the $4^15^{10}6^2$ cage. The $4^15^{10}6^2$ cage has more water molecules with a lower symmetry, which also makes it more difficult to form in the simulation due to a higher entropy penalty, which can partially explain why a higher driving force is necessary for C_2H_6 to form hydrate in the simulation. The $4^15^{10}6^2$ cage is the first cage formed in the C_2H_6 hydrate system, while the 5^{12} cage is the first cage that forms in the CH_4 system. The cage occupancy is also different when CH_4 tends to occupy small cages such as 5^{12} cages while C_2H_6 tends to occupy larger ones such as the $4^15^{10}6^2$ and $5^{12}6^2$ cages. The $4^15^{10}6^2$ cage is not common in the CH_4 system while the fraction of $5^{12}6^2$ cages is much higher though the $5^{12}6^2$ cage has two more water molecules. This can be partially explained from the moderate simulation condition in the CH_4 system. Under lower pressure or a lower degree of subcooling, the appearance of metastable cages will be less common. However, energetic preferences are always present and can also be a determining factor.

It is worthwhile to consider the comparison between the hydrate formation from the CH_4/C_2H_6 mixture system and the single component systems. Due to their small size, CH_4 tend to form the first 5^{12} cage to initiate hydrate formation. Higher pressure is needed for C_2H_6 to form hydrate in simulation. In this study, the pressure is higher than needed for the pure CH_4 system but lower than for the pure C_2H_6 system. C_2H_6 can form hydrate with the help of the hydrate-like cage structure provided from the cages formed by CH_4 . The higher

fraction of $4^15^{10}6^2$ metastable cages under high pressure shows that the cage preference for C_2H_6 forming from mixtures is the same as in the hydrate formation from pure C_2H_6 . From pure C_2H_6 , the $4^15^{10}6^2$ cage forms first and the formation of the $4^15^{10}6^2$ cage is kinetically favorable. Comparing with other types of cages, the formation of the very first cage is more independent since there are few cage-like structures around. A similar observation can also be made in the mixture system: the formation of a $4^15^{10}6^2$ metastable cage under higher pressure is more independent from the support of other cages, which is suggested by the higher fluctuation of water molecules. In other words, the $4^15^{10}6^2$ cages with C_2H_6 have lower stability, as defined by fluctuation degree, under high pressure. Since the formation of the $4^15^{10}6^2$ cages with C_2H_6 is more independent under higher pressure, resulting in more cage faces exposed to water, this is the reason for the lower stability. The decreasing in stability and the increasing in fraction is consistent with the pure C_2H_6 system where the $4^15^{10}6^2$ cage tends to form first with less independence from the surrounding cage-like structures.

However, due to the very limited information provided on the pure C_2H_6 system, there are still many aspects of interests that in the future can be explored. For instance, the question of what are the most prevalent types of cages in the C_2H_6 hydrate system remains unanswered. Barnes *et al.*^{58,59} proposed the MCG order parameter, which has been used to quantify methane hydrate nucleation and growth. This order parameter can also be used in the ethane hydrate system by modifying the parameters depending on the ethane hydrate structure. If the proper new parameters can be determined, using similar methods,⁵⁹ the critical nucleus size of ethane hydrate can be found. Then the critical nucleus sizes of methane hydrate, ethane hydrate and the binary hydrate can be compared. Hydrate should be formed under a lower

driving force with a smaller critical nucleus size. Finally, the simulation results need to be compared with experiments, though they are currently extremely challenging.

Comparing with the previous simulation studies on binary hydrates, such as CH_4/CO_2 ,⁶⁸ CH_4/THF ⁶⁹ and $\text{CH}_4/\text{H}_2\text{S}$ ^{70,71} systems, the binary $\text{CH}_4/\text{C}_2\text{H}_6$ hydrate has a main feature of interest: the concentration of C_2H_6 in water is much lower than CO_2 , THF and H_2S . Thus binary hydrate formed from a $\text{CH}_4/\text{C}_2\text{H}_6$ mixture a comparatively rarer event. Some similarities can be concluded from the studies of hydrate formation from these four binary systems. The nucleation mechanism of binary hydrate is similar to the previously developed cooperative absorption mechanism. Besides, since CH_4 is the smallest molecule and exists in all these four studies, the 5^{12} cage with CH_4 tends to form first and initiates binary hydrate nucleation.

Hydrates formed from all four binary hydrate systems have practical significances which have been discussed in Chapter 1. Since the research on these four systems focused on different aspects, many comparative analyses of these different systems are possible. The potential energy landscape of the formation of $\text{CH}_4/\text{H}_2\text{S}$ binary hydrate can be portrayed as a funnel, which is similar to the protein folding process. It is unclear whether this funnel-shaped potential energy landscape only exists in the $\text{CH}_4/\text{H}_2\text{S}$ binary hydrate system or can also be found in other systems. Whether the nonstandard cages found in the $\text{CH}_4/\text{H}_2\text{S}$ binary hydrate can also be found in other binary hydrates remain unclear. At least, in the $\text{CH}_4/\text{C}_2\text{H}_6$ binary system, I did not find these nonstandard cages. In this thesis, I discovered that trajectories with higher CH_4 concentrations have a stronger effect than for C_2H_6 to decrease the induction time. In the future, this discovery needs to be tested under different

systems. Similar to the study by Wu *et al.*, mutual effects of two guest molecules on the hydrate nucleation are also found in this thesis. In the CH₄/THF system, it is hard for THF alone to form hydrate since THF tends to occupy the large but open cages,⁶⁹ by sharing the faces from the cages formed by CH₄, THF and CH₄ can form hydrate together. More future work should also be considered on the study of the mutual effects of different molecules on hydrate nucleation.

In this thesis, the relation between cage stability, as measured by cage fluctuations, and cage selection has been first studied. The stability of different cages can reflect whether there is a large degree of hydrate cage structure that surrounds a given cage. With more protection from the cage-like structure formed by water, fewer faces are exposed to water, thus that cage should have a higher stability. Cages with different guest molecules have different stability and the stability varies with the pressure. This idea can also be tested in studies of other binary hydrates.

MD simulation has become a powerful tool in the hydrate field covering many aspects from nucleation, crystal growth and surface interactions with booming publications in recent years. Unlike macroscopic experiments, computer simulations are convenient and can provide a new vision into the microscopic world. However, the method used by most of the publications is still classical MD simulation. Though some simulation results show good agreement with experiments, new simulation methods that combine both quantum mechanics (QM) and molecular mechanics (MM) might be fruitfully applied in the future to phenomena that have a quantum character. Better agreement with experiments can thus be anticipated. Ionic effects, such as from sodium chloride, might also be investigated with the help of

QM/MM methods. Furthermore, other computational methods must be employed to study hydrate nucleation at lower thermodynamic driving forces; these methods include the path sampling methods such as Transition Path Sampling and Aimless Shooting as well as free energy calculation methods such as Umbrella Sampling^{94,96} and Equilibrium Path Sampling.^{95,96}

CH₄ and C₂H₆ are the guest molecules used in this hydrate study. In reality, the composition of guest molecules is rather complicated. Thus, the system complexity should be considered as an important factor for future study, including the simulation model for different molecules and their interactions.

As mentioned before, gas hydrate formation can also be a new method in gas transportation and separation. In these circumstances, efficient and rapid hydrate formation is necessary. Computer simulation can provide the theoretical background for such hydrate-based technologies. In industry, gas hydrate remains the main threat to flow assurance and current methods to prevent the formation of hydrate in oil and gas pipelines typically involve huge amounts of thermodynamic inhibitors such as methanol to shift the boundary of the phase diagram (lower the formation temperature of hydrate). The huge usage of thermodynamic inhibitor is expensive and not environmental friendly. The low dosage hydrate inhibitors (LDHIs) such as kinetic inhibitors and anti-agglomerants can be an effective option. However, their mechanisms of action remain unknown. Computer simulation can be used to help to understand the effects of LDHIs that act on the surface and will provide insight into developing new molecules that can be used in industry in the future.

REFERENCES

1. Sloan, E. D.; Koh, C. A. *Clathrate Hydrate of Natural Gases, 3rd ed.*; CRC Press: Boca Raton, FL, **2008**.
2. Davy, H. On Some Combinations of Oxymuriatic Gas and Oxygene, and on the Chemical Relations of These Principles, to Inflammable Bodies. *Phil Trans Roy Soc.* **1811**, 101, 1-35.
3. Carroll, J. Natural Gas Hydrates. *A Guide for Engineers, second ed.* Gulf Professional Publishing, Burlington, MA., **2009**.
4. Westbrook., G. Proceedings from the Seventh International Conference on Gas Hydrate. Heriot Watt University, Edinburgh, Scotland. **2011**.
5. Boswell.R. Is Gas Hydrate Energy within Reach? *Science*, **2009**, 325, 327-328.
6. Sloan, E. D. Fundamental Principles and Applications of Natural Gas Hydrates. *Nature*, **2003**, 426, 353-363.
7. Kennett, J. P.; Cannariato, G.; Hendy, I. L.; Behl, R. J. Methane Hydrates in Quaternary Climate Change: The Clathrate Gun Hypothesis. *Am. Geophys. Union, Washington DC*, **2003**.
8. Lyusternik.L.A. Convex Figures and Polyhedra. Dover, New York. **1963**.
9. Flegg, H. G. From Geometry to Topology. **2001**.
10. Englezos, P.; Lee, J. D. Gas Hydrates: A Cleaner Source of Energy and Opportunity for Innovative Technologies. *J. Chem. Eng.* **2005**, 22, 671-681.
11. Englezos, P. Review:Clathrate Hydrates. *Ind. Eng. Chem. Res.* **1993**, 32, 1251-1274.
12. Chandler, D. Statistical Mechanics of Isomerization Dynamics in Liquids and the Transition State Approximation. *J Chem Phys.***1978**, 68, 2959
13. Eslamimanesh, A.; Mohammadi, A. H.; Richon, D.; Naidoo, P.; Ramjugernath, D. Application of Gas Hydrate Formation in Separation Processes: A Review of Experimental Studies. *J.Chem.Thermodynamics.* **2012**, 46, 62-71.

14. Ogawa, H.; Imura, N.; Miyoshi, T.; Ohmura, R.; Mori, Y. H. Thermodynamic Simulations of Isobaric Hydrate-Forming Operations for Natural Gas Storage. *Energy & Fuels*. **23**, **2009**, 849-856.
15. Koh, C. A.; Sloan, E. D.; Sum, A. K.; Wu, D. T. Fundamentals and Applications of Gas Hydrates. *Annu. Rev. Chem. Biomol. Eng.* **2011**, *2*, 237-257.
16. Kumar, R.; Linga, P.; Englezos, P. Structure and Kinetics of Gas Hydrates from Methane/Ethane/Propane Mixtures Relevant to the Design of Natural Gas Hydrate Storage and Transport Facilities. *AIChE J.* **2008**, *54*, 2132–2144.
17. Bi, Y.; Guo, T.; Zhang, L.; Chen, L.; Sun, F. Entropy Generation Minimization for Charging and Discharging Processes in a Gas-Hydrate Cool Storage System. *Applied Energy*. **2011**, *87*, 1149–1157.
18. Uchida, T.; Ikeda, I. Y.; Takeya, S.; Kamata, Y.; Ohmura, R.; Nagao, J.; Zatsepina, O. Y.; Buffett, B. A. Kinetics and Stability of CH₄–CO₂ Mixed Gas Hydrates during Formation and Long-Term Storage. *ChemPhysChem*. **2005**, *6*, 646-654.
19. Sun, Z.; Ma, R.; Wang, R.; Guo, K.; Fa, S. Experimental Studying of Additives Effects on Gas Storage in Hydrates. *Energy & Fuels*. **2003**, *17*, 1180-1185.
20. Guo, K. H.; Shu, B. F.; Zhang, Y.; Zhao, Y. in: Proceedings of the Conference on Cryogenics and Refrigeration. **1998**, 345–348.
21. Stern, L. A.; Circone, S.; Kirby, S. H. Anomalous Preservation of Pure Methane Hydrate at 1 atm. *J. Phys. Chem. B.* **2001**, *105*, 1756-1762.
22. Seo, Y. T.; Lee, H. NMR Analysis and Gas Uptake Measurements of Pure and Mixed Gas Hydrates: Development of Natural Gas Transport and Storage Method using Gas Hydrate. *Korean J. Chem. Eng.* **2003**, *20*, 1085-1091.
23. Sabil, K. M.; Witkamp, G. J.; Peters, C. J. Phase Equilibria in Ternary (Carbon Dioxide + Tetrahydrofuran + Water) System in Hydrate-Forming Region: Effects of Carbon Dioxide Concentration and the Occurrence of Pseudo-Retrograde Hydrate Phenomenon. *J. Chem. Thermodynamics*. *42*, **2010**, 8-16.
24. Javanmardi, J.; Nasrifar, K.; Najibi, S. H.; Moshfeghian, M. Economic Evaluation of Natural Gas Hydrate as an Alternative for Natural Gas Transportation. *Applied Thermal Engineering*. **2005**, *25*, 1708-1723.

25. Mooijer-van den Heuvel, M. M.; Witteman, R.; Peters, C. J. Phase Behaviour of Gas Hydrates of Carbon Dioxide in the Presence of Tetrahydropyran, Cyclobutanone, Cyclohexane and Methylcyclohexane. *Fluid Phase Equilibria*. **2001**, 182, 97-110.
26. Chapoy, A.; Anderson, R.; Tohidi, B. Low-Pressure Molecular Hydrogen Storage in Semi-clathrate Hydrates of Quaternary Ammonium Compounds. *J. Am. Chem. Soc.* **2007**, 129, 746-747.
27. Chatti, I.; Delahaye, A.; Fournaison, L.; Petitet, J. Benefits and Drawbacks of Clathrate Hydrates: A Review of their Areas of Interest. *Energy Conversion and Management*. **2005**, 46, 1333-1343.
28. Mohammadi, A.; Eslamimanesh, A.; Belandria, V.; Richon, D. Phase Equilibria of Semiclathrate Hydrates of CO₂, N₂, CH₄, or H₂ + Tetra-n-butylammonium Bromide Aqueous Solution. *J. Chem. Eng. Data*. **2011**, 56, 3855–3865.
29. Belandria, V.; Eslamimanesh, A.; Mohammadi, A. H.; Richon, D. Gas Hydrate Formation in Carbon Dioxide+Nitrogen+Water System: Compositional Analysis of Equilibrium Phases. *Ind. Eng. Chem. Res.* **2011**, 50, 4722-4730.
30. Englezos, P.; Lee, D. Gas Hydrates: A Cleaner Source of Energy and Opportunity for Innovative Technologies. *Korean J. Chem. Eng.* **2005**, 22, 671-681.
31. Duc, N. H.; Chauvy, F.; Herri, J. M. CO₂ Capture by Hydrate Crystallization - A Potential Solution for Gas Emission of Steelmaking Industry. *Energy Conversion and Management*. **2007**, 48, 1313-1322.
32. Sun, C. Y.; Chen, G. J.; Zhang, L. W. Hydrate phase equilibrium and structure for (methane + ethane + tetrahydrofuran +water) system. *J. Chem. Thermodynamics*. **2010**, 42, 1173-1179.
33. Zhang, B. W. Thermodynamic Promotion of Tetrahydrofuran on Methane Separation from Low-Concentration Coal Mine Methane Based on Hydrate. *Energy Fuels*. **2010**, 24, 2530-2535.
34. Sugahara, T.; Haag, J. C.; Warntjes, A.; Prasad, P.; Sloan, E. D.; Koh, C. A.; Sum, A. K. Large-Cage Occupancies of Hydrogen in Binary Clathrate Hydrates Dependent on Pressures and Guest Concentrations. *J. Phys. Chem. C*. **2010**, 114, 15218-15222.

35. Makino, T.; Yamamoto, T.; Nagata, K.; Sakamoto, H.; Hashimoto, S. Thermodynamic Stabilities of Tetra-n-butyl Ammonium Chloride + H₂, N₂, CH₄, CO₂, or C₂H₆ Semiclathrate Hydrate Systems. *J. Chem. Eng. Data.* **2010**, 55, 839–841.
36. Myerson, A. D.; Trout, B. L. Nucleation from Solution. *Science.* **2013**, 341, 855-856.
37. Sosso, G. C.; Chen, J.; Cox, S. J.; Fitzner, M.; Pedevilla, P.; Zen, A.; Michaelides, A. Crystal Nucleation in Liquids: Open Questions and Future Challenges in Molecular Dynamics Simulations. *Chem. Rev.* **2016**, 116, 7078–7116.
38. Barnes, B. C.; Sum, A. K. Advances in Molecular Simulations of Clathrate Hydrates. *Curr.Opin.Chem.Eng.* **2013**, 2, 184-190.
39. Sum, A. K.; Wu, D. T.; Yasuoka, K. Energy Science of Clathrate Hydrates:Simulation-Based Advances. *MRS Bull.* **2011**, 36, 205-210.
40. Hawtin, R. W.; Quigley, D.; Rodger, P. M. Gas Hydrate Nucleation and Cage Formation at a Water/Methane Interface. *Phys.Chem.Chem.Phys.* **2008**, 10, 4853-4864.
41. Zhang, J.; Hawtin, R. W.; Yang, Y.; Nakagawa, E.; Rivero, M.; Choi, S. K.; Rodger, P. M. Molecular Dynamics Study of Methane Hydrate Formation at a Water/Methane Interface. *J.Phys.Chem.B.* **2008**, 112, 10608-10618.
42. Sakamaki, R.; Sum, A. K.; Narumi, T.; Ohmura, R.; Yasuoka, K. Thermodynamic Properties of Methane/Water Interface Predicted by Molecular Dynamics Simulations. *J.Chem.Phys.* **2011**, 134, 144702-144117.
43. Anderson, B. J.; Tester, J. W.; Borghi, G. P.; Trout, B. L. Properties of Inhibitors of Methane Hydrate Formation via Molecular Dynamics Simulations. *J. Am. Chem. Soc.* **2005**, 127, 17852.
44. Yagasaki, T.; Matsumoto, M.; Tanaka, H. Adsorption Mechanism of Inhibitor and Guest Molecules on the Surface of Gas Hydrates. *J. Am. Chem. Soc.* **2015**, 137, 12079–12085.
45. Yagasaki, T.; Matsumoto, M.; Tanaka, H. Mechanism of Slow Crystal Growth of Tetrahydrofuran Clathrate. *J.Chem.Phys.C.* **2016**, 120, 3305-3313.
46. Yagasaki, T.; Matsumoto, M.; Tanaka, H. Formation of Clathrate Hydrates of Water-Soluble Guest Molecules. *J.Chem.Phys.C.* **2016**, 120, 21512–21521.

47. Christensen, R.; Sloan, E. D. Mechanisms and Kinetics of Hydrate Formation. *Ann.N.Y.Acad.Sci.* **1994**, 175, 283–305.
48. Sloan, E. D.; Fleyfel, F. A. Molecular Mechanism for Gas Hydrate Nucleation from Ice. *AIChE J.* **1991**, 37, 1281–1292.
49. Radhakrishnan, R.; Trout, B. L. A New Approach for Studying Nucleation Phenomena Using Molecular Simulations: Application to CO₂ Hydrate Clathrates. *J.Chem.Phys.* **2002**, 117, 1786-1796.
50. Moon, C.; Taylor, P. C.; Rodger, P. M. Molecular Dynamics Study of Gas Hydrate Formation. *J.Am.Chem.Soc.* **2003**, 125, 367-382.
51. Guo, G. J.; Li, M.; Zhang, Y. G.; Wu, C. H. Why can Water Cages Adsorb Aqueous Methane? A Potential of Mean Force Calculation on Hydrate Nucleation Mechanisms. *Phys.Chem.Chem.Phys.* **2009**, 11, 10427-10437.
52. Jacobson, L. C.; Hujo, W.; Molinero, V. Amorphous Precursors in the Nucleation of Clathrate Hydrate. *J.Am.Chem.Soc.* **2010**, 132, 15065-15072.
53. Jacobson, L. C.; Hujo, W.; Molinero, V. Nucleation Pathways of Clathrate Hydrate: Effect of Guest Size and Solubility. *J.Phys.Chem.B.* **2010**, 114, 13796-13807.
54. Walsh, M. R.; Koh, C. A.; Sloan, E. D.; Sum, A. K.; Wu, D. T. Microsecond Simulation of Spontaneous Methane Hydrate Nucleation and Growth. *Science.* **2009**, 326, 1095-1098.
55. Bi, Y. F.; Li, T. S. Probing Methane Hydrate Nucleation through the Forward Flux Sampling Method. *J.Phys.Chem.B.* **2014**, 118, 13324-13332.
56. Moon, C.; Hawtin, R. W.; Rodger, P. R. Nucleation and Control of Clathrate Hydrates: Insights from Simulation. *Faraday Discuss.* **2007**, 136, 367-382.
57. Jacobson, L. C.; Matsumoto, M.; Molinero, V. Order Parameters for the Multistep Crystallization of Clathrate Hydrates. *J.Chem.Phys.* **2011**, 135, 074501.
58. Barnes, B. C.; Beckham, G. T.; Wu, D. T.; Sum, A. K. Two-component Order Parameter for Quantifying Clathrate Hydrate Nucleation and Growth. *J.Chem.Phys.* **2014**, 140, 164506.
59. Barnes, B. C.; Knott, B. C.; Beckham, G. T.; Wu, D. T.; Sum, A. K. Reaction Coordinate of Incipient Methane Clathrate Hydrate Nucleation. *J.Phys.Chem.B.* **2014**, 118, 13236-13243.

60. Bai, D.; Chen, G. J.; Zhang, X. W. Microsecond Molecular Dynamics Simulations of the Kinetic Pathways of Gas Hydrate Formation from Solid Surfaces. *Langmuir*. **2011**, 27, 5961-5967.
61. Vatamanu, J.; Kusalik, P. G. Molecular Insights into the Heterogeneous Crystal Growth of sI Methane Hydrate. *J. Phys. Chem. B*. **2006**, 110, 15896-15904.
62. Walsh, M. R.; Beckham, G. T.; Koh, C. A.; Sloan, E. D.; Wu, D. T.; Sum, A. K. Methane Hydrate Nucleation Rates from Molecular Dynamics Simulations: Effects of Aqueous Methane Concentration, Interfacial Curvature, and System Size. *J. Phys. Chem. C*. **2011**, 115, 21241-21248.
63. Walsh, M. R.; Rainey, J. D.; Lafond, P. G.; Park, D. H.; Beckham, G. T.; Jones, M. D.; Lee, K. H.; Koh, C. A.; Sloan, E. D.; Wu, D. T.; Sum, A. K. The Cages, Dynamics, and Structuring of Incipient Methane Clathrate Hydrates. *Phys. Chem. Chem. Phys.* **2011**, 13, 19951-19959.
64. Liang, S.; Kusalik, P. G. Nucleation of Gas Hydrates within Constant Energy Systems. *J. Phys. Chem. B*. **2013**, 117, 1403-1410.
65. Zhang, Z.; Walsh, M. R.; Guo, G. J. Microcanonical Molecular Simulations of Methane Hydrate Nucleation and Growth: Evidence that Direct Nucleation to sI Hydrate is among the Multiple Nucleation Pathways. *Phys. Chem. Chem. Phys.* **2015**, 17, 8870-8876.
66. Brumby, P. E.; Yuhara, D.; Wu, D. T.; Sum, A. K.; Yasuoka, K. Cage Occupancy of Methane Hydrates from Gibbs Ensemble Monte Carlo Simulations. *Fluid Phase Equilibria*. **2016**, 413, 242-248.
67. Liu, C.; Zhang, Z.; Guo, G. J. Effect of Guests on the Adsorption Interaction between a Hydrate Cage and Guests. *RSC Adv*. **2016**, 6, 106443.
68. He, Z. J.; Gupta, K. m.; Linga, P.; Jiang, J. W. Molecular Insights into the Nucleation and Growth of CH₄ and CO₂ Mixed Hydrates from Microsecond Simulations. *J. Phys. Chem. C*. **2016**, 120, 25225-25326.
69. Wu, J. Y.; Chen, L. J.; Chen, Y.; Lin, S. T. Molecular Dynamics Study on the Nucleation of Methane+Tetrahydrofuran Mixed Guest Hydrate. *Phys. Chem. Chem. Phys.* **2016**, 18, 9935-9947.
70. Hall, K. W.; Carpendale, S.; Kusalik, P. G. Evidence from Mixed Hydrate Nucleation for a Funnel Model of Crystallization. *Proc. Natl. Acad. Sci. U.S.A.* **2016**, 113, 12041-12046.

71. Hall, K. W.; Zhang, Z.; Kusalik, P. G. Unraveling Mixed Hydrate Formation: Microscopic Insights into Early Stage Behavior. *J.Phys.Chem.B.* **2016**, 120, 13218-13223.
72. Lee, J. D.; Susilo, R.; Englezos, P. Methane-Ethane and Methane-Propane Hydrate Formation and Decomposition on Water Droplets. *Chem.Eng.Sci.* **2005**, 60, 4203-4212.
73. Subramanian, S.; Kini, R. A.; Dec, S. F.; Sloan, E. D. Evidence of Structure II Hydrate Formation from Methane+Ethane Mixtures. *Chem.Eng.Sci.* **2000**, 55, 1981-1999.
74. Subramanian, S.; Ballard, A. L.; Kini, R. A.; Dec, S. F.; Sloan, E. D. Structural Transitions in Methane+Ethane Gas Hydrates-Part I: Upper Transition Point and Applications. *Chem.Eng.Sci.* **2000**, 55, 5763-5771.
75. Ohno, H.; Strobel, T. A.; Dec, S. F.; Sloan, E. D.; Koh, C. A. Raman Studies of Methane-Ethane Hydrate Metastability. *J.Phys.Chem.A.* **2009**, 113, 1711-1716.
76. Naeiji, P.; Mottahedin, M.; Varaminian, F. Separation of Methane-Ethane Gas Mixtures via Gas Hydrate Formation. *Separation and Purification Technology.* **2014**, 123, 139-144.
77. Schicks, J. M.; Luzi-Helbing, M. Cage Occupancy and Structural Changes during Hydrate Formation from Initial Stages to Resulting Hydrate Phase. *Spectrochim.Acta,Part A.* **2013**, 115, 528-536.
78. Schicks, J. M.; Luzi-Helbing, M. Kinetic and Thermodynamic Aspects of Clathrate Hydrate Nucleation and Growth. *J.Chem.Eng.Data.* **2014**, 60, 269-277.
79. Katz, D. L.; Cornell, D.; Vary, J. A.; Kobayashi, R. E. R.; Poettmann, F. H.; Weinaug, C. F. Handbook of Natural Gas Engineering. *New York:McGraw-Hill,Book,Company,Inc.* **1959**.
80. Wilson, D. T.; Barnes, B. C. W. T.; Sum, A. K. Molecular dynamics simulations of the Formation of Ethane Clathrate Hydrates. *Fluid Phase Equilib.* **2016**, 413, 229-234.
81. Hess, B.; Kutzner, C.; van der Spoel, D.; Lindahl, E. Gromacs 4:Algorithms for Highly Efficient,Load-Balanced,and Scalable Molecular Simulation. *J.Chem.Theory Comput.* **2008**, 4, 435-447.
82. Abascal, J. L. F.; Sanz, E.; Fernandez, R. G.; Vega, C. A Potential Model for the Study of Ices and Amorphous Water: TIP4P/Ice. *J.Chem.Phys.* **2005**, 122, 234511.
83. Jorgensen, W. L.; Madura, J. D.; Swenson, C. J. Optimized Intermolecular Potential Functions for Liquid Hydrocarbons. *J.Am.Chem.Soc.* **1984**, 106, 6638-6646.

84. Humphrey, W.; Dalke, A.; Schulten, K. VMD: Visual Molecular Dynamics. *J.Molec.Graph.* **1996**, 14, 33-38.
85. Guo, G. J.; Rodger, P. M. Solubility of Aqueous Methane under Metastable Conditions: Implications for Gas Hydrate Nucleation. *J.Phys.Chem.B.* **2013**, 117, 6498-6504.
86. Tung, Y. T.; Chen, L.; Chen, Y. P.; Lin, S. T. The Growth of Structure I Methane Hydrate from Molecular Dynamics Simulations. *J. Phys. Chem. B.* **2010**, 114, 10804–10813.
87. Tung, Y. T.; Chen, L. J.; Chen, Y. P.; Lin, S. T. In Situ Methane Recovery and Carbon Dioxide Sequestration in Methane Hydrates: A Molecular Dynamics Simulation Study. *J. Phys. Chem. B.* **2011**, 115, 15295–15302.
88. English, N. J.; MacElroy, J. M. D. Theoretical Studies of the Kinetics of Methane Hydrate Crystallization in External Electromagnetic Fields. *J. Chem. Phys.* **2004**, 120, 10247-10249.
89. English, N. J.; Taylor, J. K. Molecular-Dynamics Simulations of Methane Hydrate Dissociation. *J. Chem. Phys.* **2005**, 123, 244503-244516.
90. Jacobson, L. C.; Hujo, W.; Molinero, V. Thermodynamic Stability and Growth of Guest-Free Clathrate Hydrates: A Low-Density Crystal Phase of Water. *J.Phys.Chem.B.* **2009**, 113, 10298-10307.
91. Liu, J.; Hou, J.; Xu, J.; Liu, H.; Chen, G.; Zhang, J. Formation of Clathrate Cages of sI Methane Hydrate Revealed by ab initio Study. *Energy.* **2016**, 120, 1-7.
92. Jiménez-Ángeles, F.; Firoozabadi, A. Nucleation of Methane Hydrates at Moderate Subcooling by Molecular Dynamics Simulations. *J.Phys.Chem.C.* **2014**, 118, 11310-11318.
93. He, Z.; Linga, P.; Jiang, J. What are the Key Factors Governing the Nucleation of CO₂ Hydrate. *Phys.Chem.Chem.Phys.* **2017**, 19, 15657-15661.
94. Torrie, G.; Valleau, J. Nonphysical Sampling Distributions in Monte Carlo Free-Energy Estimation: Umbrella Sampling. *J Comp Phys.* **1977**, 23, 187-199.
95. Peters, B.; Zimmerman, N. E. R.; Beckham, G. T.; Tester, J. W.; Trout, B. L. Path Sampling Calculation of Methane Diffusivity in Natural Gas Hydrates from a Water-Vacancy Assisted Mechanism. *J.Am.Chem.Soc.* **2008**, 130, 11342-11350.

96. Frenkel, D; Smit, B.; Understanding Molecular Simulation: From Algorithms to Applications. *Academic Press, San Diego, 1996*